Journal of Structural Geology 33 (2011) 1662–1680

Contents lists available at SciVerse ScienceDirect

Journal of Structural Geology

journal homepage: www.elsevier.com/locate/jsg

The fracture pattern of the Sant Corneli Bóixols oblique inversion anticline (Spanish Pyrenees)

S. Tavani*, J. Mencos, J. Bausà, J.A. Muñoz

Geomodels, Departament de Geodinàmica i Geofísica, Facultat de Geologia, Universitat de Barcelona, c/Martí Franquès s/n, 08028 Barcelona, Spain

ARTICLE INFO

Article history:
Received 26 January 2011
Received in revised form
13 August 2011
Accepted 23 August 2011
Available online 29 August 2011

Keywords:
Fracture
Inversion
Folding
Transpression

ABSTRACT

In this work we present and discuss the macro and mesostructural deformation patterns of the Late Cretaceous Sant Corneli Bóixols oblique inversion anticline (Spanish Pyrenees). This E–W striking and south-verging structure developed by inversion of an Early Cretaceous extensional fault system, formed by WNW–ESE striking faults (oriented perpendicular to the Early Cretaceous stretching direction) and transfer faults. During inversion, the shortening direction was oriented NNW–SSE, i.e. oblique to both basin margin and inherited extensional deformation structures. A pre to early-folding layer-parallel shortening (LPS) stage caused the strike-slip reworking of inherited extensional structures and the development of extensional and contractional structures oriented parallel and perpendicular to the shortening direction, respectively. Few faults clearly developed during the late stages of fold growth, in response to a stress field having principal axes parallel to those of the layer-parallel shortening event, i.e. oblique to the fold axis. WSW–ENE striking bedding-perpendicular joints and veins postdate the LPS pattern and can be associated with a syn-folding layer-parallel stretching. Analogously, few reverse faults having a top-to-the crest shear sense are associated with flexural-slip folding. Both layer-parallel stretching and shear sense provided by flexural-slip related elements are not perpendicular to the fold axial trend. All these assemblages were overprinted by a set of post-folding extensional structures oriented oblique to the strike of the anticline.

Presented data show that syn-inversion fractures in the Sant Corneli Bóixols Anticline are neither parallel nor perpendicular to the fold axial trend, and their development has been controlled by inherited extensional structures and the regional shortening direction.

1. Introduction

The type, frequency and orientation of fractures developed during or immediately before folding depend on several parameters. These include, among the others, the mechanical stratigraphy (e.g. Corbett et al., 1987; Gross, 1995; Fischer and Jackson, 1999; Chester, 2003; Tavani et al., 2008), the environmental conditions (like temperature, pressure, water circulation; e.g. Engelder and Marshak, 1985; Chester et al., 1991; Jamison, 1992; Lemiszki et al., 1994), and the presence of inherited fracture patterns (e.g. Bergbauer and Pollard, 2004; Bellahsen et al., 2006), and the stress field (e.g. Fletcher and Pollard, 1981; Hancock, 1985; Engelder, 1987; Pollard and Aydin, 1988; Angelier, 1994). Since the pioneering work of Stearns (1968), several studies have documented the existence of rather constant angular relationships between fold axial trend and fractures in reservoir-scale thrust-related anticlines (e.g. Mitra and Yonkee, 1985; Price and Cosgrove, 1990; Cooper, 1992; Lemiszki et al., 1994; Tavani et al., 2006). In the absence of inherited sets, in fact, fractures commonly include elements striking parallel and perpendicular to the fold axis, and conjugate strike-slip faults whose bisectors are parallel and perpendicular to the fold axial trend. The documented variability of fracture attributes, both across- (e.g. Srivastava and Engelder, 1990; Tavani et al., 2008) and along-strike (e.g. Tavani et al., 2006; Savage et al., 2010), indicates that the folding process is able to modify the remote stress field and, thus, can influence the development of fractures.

The growth of thrust-related anticlines can occur by limb rotation about fixed axial surfaces (e.g. De Sitter, 1956) or by lateral migration of active axial surfaces (e.g. Ramsay, 1974; Suppe, 1983). In both cases, layer bending is facilitated by (1) flexural folding (Donath and Parker, 1964), i.e. slip between layers (flexural-slip) or flow within layers (flexural flow), and (2) tangential-longitudinal strain (Ramsay, 1967). The orientation of fractures associated with flexural folding depends on the flexural-slip/flow shear direction

* Corresponding author. Tel.: +34 93 403 5957.
E-mail address: stefano.tavani@ub.edu (S. Tavani).

0191-8141/$ – see front matter © 2011 Elsevier Ltd. All rights reserved.
doi:10.1016/j.jsg.2011.08.007

(e.g. Anastasio et al., 1997; Engelder and Peacock, 2001). Tangential-longitudinal strain is expected to produce fractures striking parallel to the axial surface (e.g. Turcotte and Schubert, 1982; Price and Cosgrove, 1990; Srivastava and Engelder, 1990; Lemiszki et al., 1994). How these syn-folding patterns are influenced by the regional stress field is difficult to decipher in roughly cylindrical structures striking perpendicular to the regional shortening direction. In these cases the regional shortening direction is parallel to both tangential-longitudinal strain and flexural-slip/flow shear direction.

Inversion structures permit to bypass this problem. During basin inversion the compression direction is, in the general case, oblique to the strike of the inherited structures (which controls the orientation of the inversion-related ones; e.g. Casas-Sainz, 1993; Thomas and Coward, 1995; Brun and Nalpas, 1996). This obliquity allows evaluation of the contributions of regional and folding-related stress fields in determining the orientation of syn-folding fractures, which is the aim of this work.

We present and discuss the macro and mesostructural deformation pattern of the Sant Corneli Bóixols Anticline (Spanish Pyrenees). This E–W striking and south-verging anticline developed during Late Cretaceous, inverting an Early Cretaceous normal fault system (e.g. Bond and McClay, 1995; García-Senz, 2002; Muñoz, 2002). About 1600 mesostructural data were collected in the anticline, both along major map-scale faults and in areas far from these macrostructures. In the first set of field sites we analysed the kinematics of the map-scale faults. In the second set we collected data about the "background" deformation pattern, with a random data collection criterion allowing to reduce the bias between the outcrop fracture population and its sampled part (Tavani et al., 2010).

In the Sant Corneli Bóixols Anticline we recognised three deformational stages: Early Cretaceous extension, Late Cretaceous inversion, and Cenozoic post-folding extension. Deformation structures developed from early-inversion to post-folding extension are neither parallel nor perpendicular to the fold axis, which has important implications for syn-folding fracturing models and folding mechanisms.

2. Geological setting

The Sant Corneli Bóixols Anticline is located at the front of the Bóixols thrust sheet (Fig. 1a), which corresponds to the uppermost of the upper thrust sheets of the central Pyrenees (e.g. Muñoz, 2002). The anticline is a result of Late Cretaceous inversion of an earlier system of extensional basins (Bond and McClay, 1995; García-Senz, 2002; Muñoz, 2002), where the accumulation of Lower Cretaceous syn-rift sediments in the hangingwall of the normal faults exceeded 4 km, while it was strongly reduced or even absent in the footwall (García-Senz, 2002).

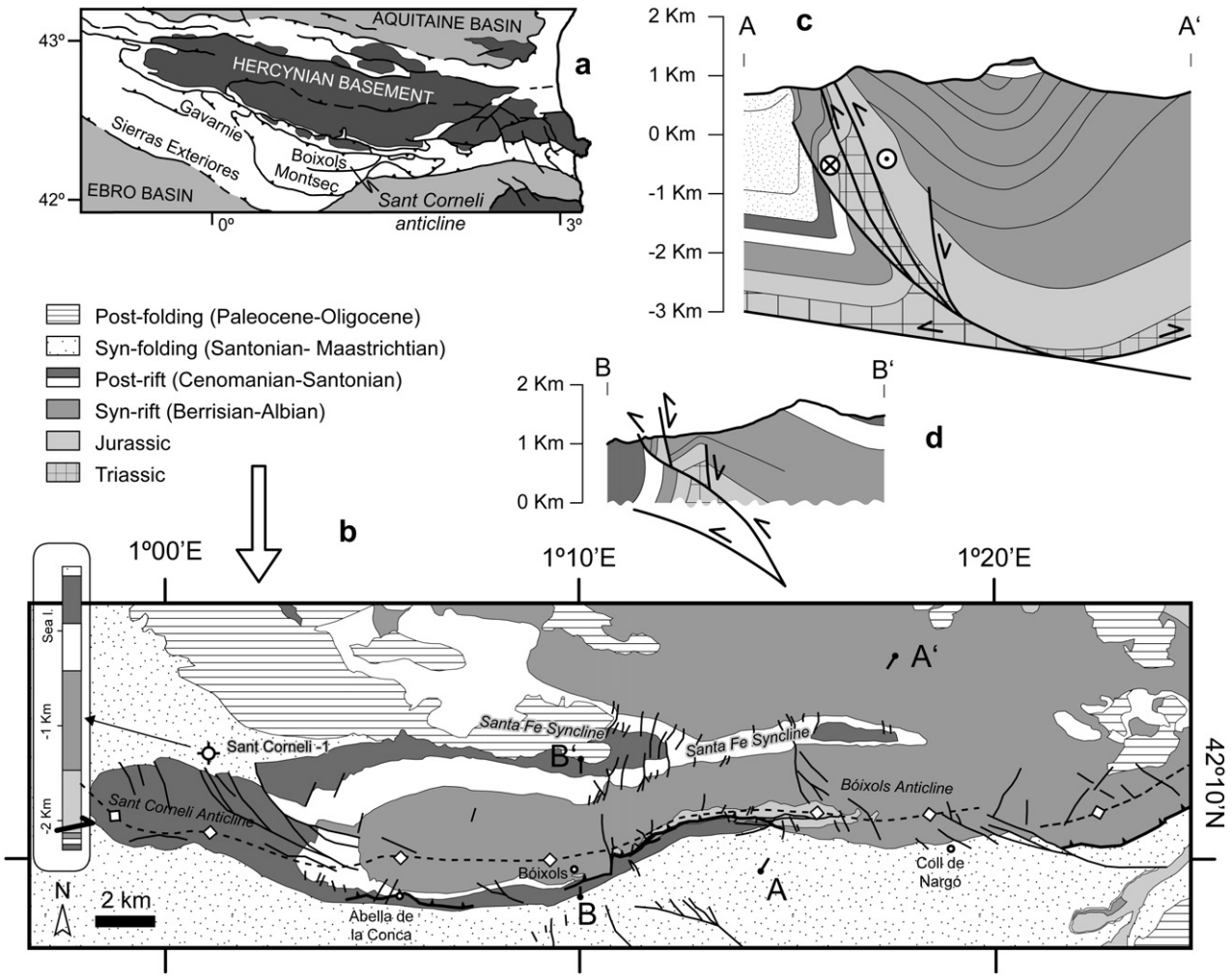

Fig. 1. Geological maps (a, b) and cross-sections (c, d) (modified from Dinares-Turell and Garcia-Senz, 2000; García-Senz, 2002) of the Sant Corneli Bóixols Anticline.

The Bóixols thrust sheet is characterised by a set of synclines and anticlines roughly striking E–W, the Santa Fe Syncline and the Sant Corneli Bóixols Anticline being the major ones (Fig. 1b). The folded multilayer can be divided in five groups (Simó, 1986; Cuevas, 1992; García-Senz, 2002; Beamud et al., 2003) (Fig. 1b): (1) Post-folding clays, sandstones and conglomerates (Lower Paleocene to Oligocene); (2) Syn-folding quartzitic and calcareous sandstones, marls, clays and turbidites (Upper Santonian to Maastrichtian); (3) Pre-folding and post-rift calcarenites, limestones and marls (Upper Cenomanian to Lower Santonian); (4) syn-rift limestones, marls, and clays (Tithonian/Berriasian to Upper Albian); (5) Pre-rift limestones and dolostones (Jurassic) and evaporites (Keuper, Triassic). Geometrical relationships between Upper Cretaceous syn-folding and pre-folding layers indicate that the main folding episode took place during Late Cretaceous, when the forelimb reached a near-vertical attitude. However, a younger Cenozoic reactivation has occurred, as indicated by the fact that in the northern limb of the study anticline, Paleocene to Oligocene conglomerates dip about 20° towards the north and show growth geometries.

The studied anticline is divided in two sectors: Sant Corneli Anticline to the west and Bóixols Anticline to the east (Fig. 1b). It is characterised by an overall E–W striking and westward plunging axis that includes segments with different orientations (Fig. 1b). The fold shape is rounded and asymmetric. Bedding dip across the fold progressively passes from 30 to 40° in the northward dipping backlimb up to 90° (locally overturned) in the southward dipping forelimb. In the central portion of the anticline the backlimb overthrusts the near-vertical/overturned forelimb and as a result in this area the crestal sector is not exposed.

Map-scale faults are present all along the anticline. Right-lateral WNW–ESE striking faults locate in the western and eastern sectors. In the western sector they display a polyphasic history (right-lateral + normal) that will be discussed later in detail. From these faults emanate NNW–SSE striking normal faults. NNE–SSW striking normal faults are located all along the anticline and also affect the Santa Fe syncline. The forelimb of the anticline is affected by low-dipping thrusts, which developed during late stages of the fold growth. The main thrust is buried and was encountered at about 2100 m b.s.l. in the Sant Corneli-1 well (Fig. 1b) (Lanaja, 1987). It mostly reworked the main normal fault system, as indicated by the facts that: (1) In the central portion of the anticline (where Jurassic sediments are exposed) the Lower Cretaceous sediments thickness is strongly reduced in the forelimb (with respect to both crest and backlimb); (2) In the eastern sectors, to the south of the anticline (Fig. 1b), the Lower Cretaceous sediment thickness is strongly reduced with respect to the northern limb of Bóixols Anticline; (3) In the Sant Corneli-1 well the hangingwall of the thrust includes a thick portion of Lower Cretaceous syn-rift sediments while the overturned sedimentary sequence of the footwall includes only a thin portion of Lower Cretaceous rocks.

In the Bóixols Anticline, isopachs distribution of Lower Cretaceous sediments indicates that the basin was roughly E–W elongated (García-Senz, 2002). Proceeding towards the west, in the Sant Corneli Anticline and more to the west, these isopachs attain a WNW–ESE orientation, indicating that the basin was WNW–ESE elongated (Mencos, 2011).

3. Data

Data about joints, veins, pressure solution cleavages, faults and fault-related deformation structures were collected in 53 sites, mostly located in the central and western sectors of the anticline. Mesoscale deformation structures were characterised by their type, orientation, overprinting relationships and orientation of the reference bedding, which allowed us to analyse data after restoring the bedding surface to the horizontal. At 10 sites we determined the kinematics of the major map-scale faults by analysing the geometry and the overprinting relationships of kinematic indicators (i.e. slickenlines and fault-related deformation structures; e.g. Doblas, 1998) (Fig. 2). Two other sites deserved a particular attention, due to the presence of well-developed Lower Cretaceous syn-rift mesostructures. At sites located in areas far from map-scale faults we analysed the "background" mesoscale deformation pattern. Most of these sites have a minimum across-fault distance from map-scale faults of 70–100 m. Few are closer, however, they are clearly outside the damage zone of map-scale faults.

Fault rotax was used, together with slickenlines, to analyse fault data. The rotax is the direction lying along the fault plane and striking perpendicular to the slickenline direction (Fig. 2A) (e.g. Wise and Vincent, 1965). We used this derived measure as it is particularly useful in stereoplots. The rotaxes tend to cluster around a vertical direction for steeply dipping strike-slip faults, regardless of the fault strike, thus allowing to immediately distinguish between strike-slip and dip-slip fault systems. Rotaxes of dip-slip faults cluster along the direction perpendicular to the shear direction, regardless of the fault dip, which instead affects the clustering of slickenlines. Another advantage of rotax is that it allows to easily recognise conjugate fault systems in stereoplots. In most cases, the intersection of newly formed conjugate faults corresponds to the $\sigma 2$ direction, implying that slickenlines lie along the $\sigma 1$–$\sigma 3$ plane. Accordingly, in these cases the rotax (i.e. slickenline normal) is also parallel to the $\sigma 2$ direction. The result is that such a conjugate fault system has rotaxes clustered around the intersection between the two conjugate fault sets (Fig. 2B). Notice that a pre-folding conjugate dip-slip fault system in horizontally bedded strata has rotaxes that lie within the bedding planes; this relationship also holds if bedding and faults rotate due to folding. Thus the rotax represents a useful object in a folded layer to "graphically" distinguish between pre-folding systems whose rotaxes lie within the bedding plane (Fig. 2C) and post-folding conjugate system whose rotaxes lie outside of the bedding plane.

3.1. Map-scale faults

WNW–ESE striking faults are exposed in the eastern and western sectors of the Sant Corneli Bóixols Anticline (sites from 1 to 5 of Fig. 3). At the transition between the Sant Corneli and the Bóixols anticlines, this fault set includes a major system located in the crest (Fig. 3B, sites from 1 to 3). In its western and central sectors this fault system has a right-lateral strike-slip kinematics (Fig. 3B sites 1 and 2; Fig. 3C), while more to the east it is extensional and offsets an NNE–SSW striking normal fault (Fig. 3B site 3; Fig. 3D). In the eastern sector of the anticline, WNW–ESE striking right-lateral faults displace near-vertical beds in the forelimb (Fig. 3 sites 4 and 5), indicating a late to post-folding development.

In the Sant Corneli Anticline, syn-folding NNW–SSE striking extensional faults emanate from WNW–ESE striking right-lateral faults (Fig. 3 site 6), resembling an extensional horsetail termination of the WNW–ESE right-lateral system.

In the central and eastern portions of the anticline the near-vertical forelimb is affected by low-displacement north-dipping thrusts (Fig. 4 sites from 7 to 9). These thrusts are SSE- to SE-directed (Fig. 4 sites 7 and 9a; Fig. 4C) and displace near-vertical beds, indicating a late-folding development. Many of these reverse faults have been later reactivated, as indicated by mesostructures providing both top-to-the north (Fig. 4D) and top-to-the west shear senses (Fig. 4 site 8). In the central sector of the structure one of these thrusts is offset of few tens of metres by an NNW–SSE striking and WSW-dipping extensional fault (Fig. 4 site 9b).

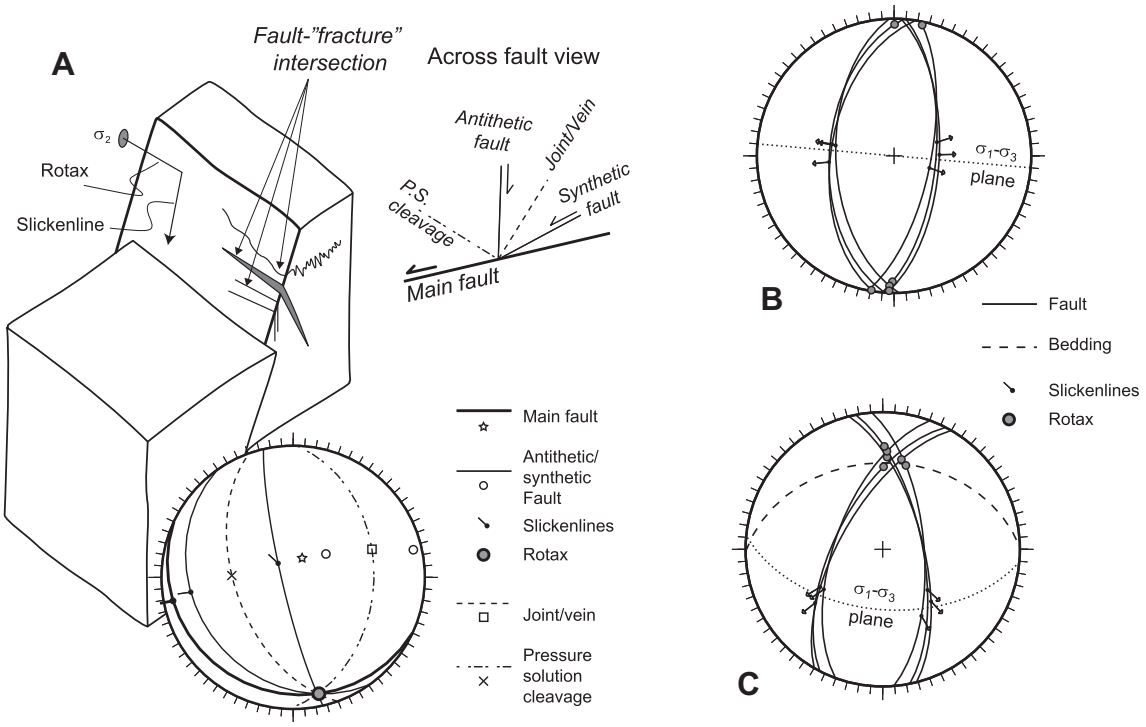

Fig. 2. (A) 3D block diagram, across-fault section and stereoplot illustrating the relationships between fault geometry and kinematics and fault-related deformation structures. (B) Stereoplot of conjugate normal faults with rotaxes clustering at the intersection between the two fault sets. (C) Tilted conjugate normal faults with rotaxes clustering at the intersection between fault sets and bedding surface.

The last set of map-scale faults is represented by NNE–SSW striking extensional faults, which affect the forelimb and the backlimb of the Sant Corneli and Bóixols anticlines and the Santa Fe syncline (Fig. 5 sites 10 and 11). In the backlimb this fault system includes normal faults dipping about 60° towards both WNW and ESE (Fig. 5 site 11). As the rotaxes of these faults are sub-horizontal and do not lie along bedding, they have been interpreted as a post-folding conjugate normal fault system. In the forelimb this system includes both NNE–SSW striking faults dipping about 60° towards WNW and low-angle normal faults (Fig. 5 site 10; Fig. 5C). In both cases rotaxes are low-dipping or sub-horizontal, while bedding dip ranges from 50° to near vertical.

Two sites located close to the Bóixols village (Figs. 6 and 7) are of particular interest, although they are not located along a map-scale fault. In the first outcrop (Fig. 6), the tectonic and stratigraphic boundaries between Lower Cretaceous syn-rift sediments and Jurassic pre-rift sediments are well exposed (Fig. 6B). Near vertical and WNW–ESE striking layers of Lower Cretaceous sediments overly N–S striking and westward dipping Jurassic limestones, which are in the footwall of a set of normal faults having the Lower Cretaceous sediments in the hangingwall (Fig. 6B). Mesostructural observations (Fig. 6C) and geometrical relationships between Jurassic and Lower Cretaceous sediments indicate an evolution including three stages, which is summarised in Fig. 6D. During the Early Cretaceous, a set of transversal NE–SW striking conjugate normal faults developed in Jurassic limestones. These faults, together with Jurassic layers, then rotated about an NE–SW striking horizontal axis synchronously with the deposition of Lower Cretaceous sediments. One of the two sets of rotated normal faults has been later reworked as thrusts, which led to the local development of pervasive pressure solution cleavage in the Lower Cretaceous sediments. Finally, the entire system rotated during folding about an E–W striking axis.

In the second outcrop (Fig. 7), the geometry and kinematics of the Lower Cretaceous extensional mesostructures were studied (Fig. 7). The presence of soft-sediment deformation structures (Fig. 7a), syn-faulting sediment geometries (Fig. 7b), and syn-tectonic slump intervals with clasts hosting pre-slump fractures (Fig. 7c,d), highlights that the Early Cretaceous extensional event is well registered in this site. The inferred Early Cretaceous stretching direction is approximately NNE–SSW, as indicated by normal faults mostly striking from NW–SE to E–W (Fig. 7e), which include some clearly syn-sedimentary faults. Most of these faults have been later reworked as right-lateral strike-slip faults.

3.2. Meso-scale deformation pattern

41 field sites are located far from map-scale faults and allowed us to analyse the "background" mesoscale deformation pattern (Fig. 8a). In the Cenozoic portion of the multilayer data have been collected in poorly layered conglomerates. In these sediments the deformation pattern includes: (1) two sets of conjugate normal faults striking about NW–SE; (2) two sets of joints roughly perpendicular to bedding and striking parallel and perpendicular to the normal faults, respectively (Fig. 8b). All these elements are not stratabound.

Data in the post and syn-rift sediments have been collected in layered limestones (Cenomanian to Santonian post-rift sediments) and well-layered marly limestones (syn-rift sediments). Joints, veins, and pressure solution cleavages are mostly stratabound, while faults include both stratabound and, mostly, not stratabound elements. Data collected in the post and syn-rift rocks are shown in their present orientation (Unrotated insets of Fig. 8) and after restoring the bedding dip to the horizontal (Rotated insets of Fig. 8).

In their present orientation, poles to faults in the post-rift rocks are rather scattered (Fig. 8c), while in the rotated projection four main maxima can be recognised (Fig. 8d), corresponding to planes near perpendicular to bedding and striking N105°, N130° and N195°, and planes striking N150° and dipping about 65° towards the SW. Fault rotaxes are also better clustered in the

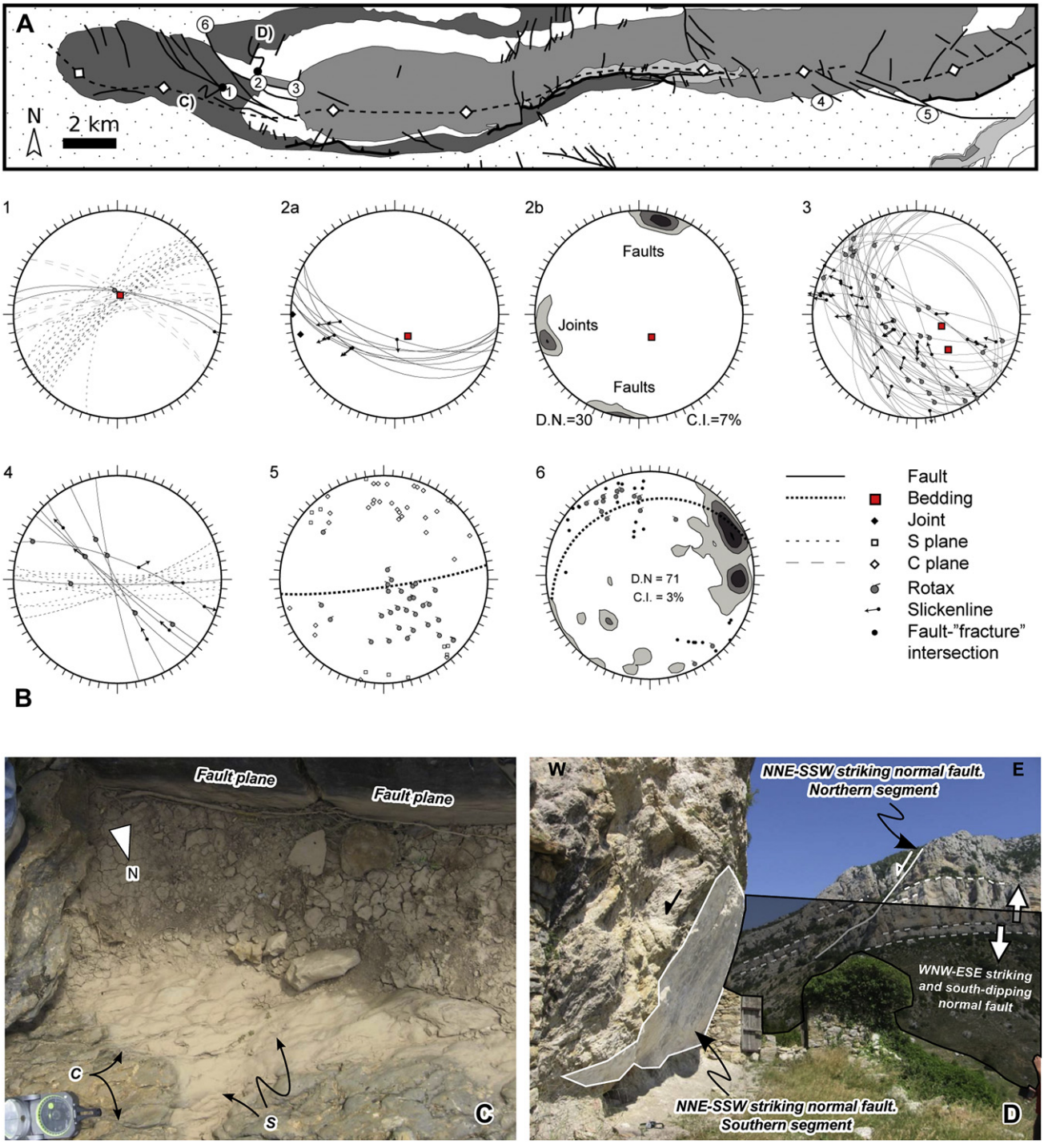

Fig. 3. Map-scale analysis of WNW–ESE and NNW–SSE striking faults. (A) Location of sites and photos. (B) Stereoplots. In the contouring D.N. and C.I. indicate data number and contouring intervals, respectively. The mesostructural pattern observed in site 1 is that of a purely right-lateral strike-slip fault, the fault plane and the associated S and C structures being near vertical and perpendicular to bedding. In site 2, data from the fault plane (site 2a) indicate a right-lateral transtensional kinematics, with a younger dip-slip extensional movement. In the same site, the fault damage zone is characterised by the pervasive presence of faults striking parallel to the major one and joints striking about NNW SSE (site 2b), indicating again a mostly right-lateral behaviour. Site 3 locates in the damage zone of the WNW–ESE striking fault, where mesofaults strike NW–SE and N–S and dip towards the west. Their kinematics are normal and slickenlines are clustered around two maxima indicating two shear events: top-to-SW and top-to-W, the second one being the older. In this site there is also a third set of faults striking about WNW–ESE and perpendicular to the bedding surface, which displays a right-lateral kinematics. The faults of sites 4 and 5 display a right-lateral kinematics, as indicated by slickenlines, and C and S structures, striking WNW–ESE and about E–W, respectively. Site 6 locates at the northern termination of a major NNW–SSE striking fault. Here poles to mesofaults are mostly clustered around two maxima, corresponding to planes dipping 80° towards the west and striking N150° and N180°, respectively. The direction of fault rotaxes and fault-fracture intersection (both of them corresponding to the direction lying on the fault plane and perpendicular to the slip direction; Fig. 2) is mostly NNW–SSE. Part of them roughly lie along the bedding surface, however the most are sub-horizontal, indicating both pre and, mainly, post-tilting activity (i.e. a syn-folding development), being the stretching direction WSW–ENE. (C) S–C structures of site 1. (D) WNW–ESE striking normal fault displacing an NNE–SSW striking normal fault (site 3).

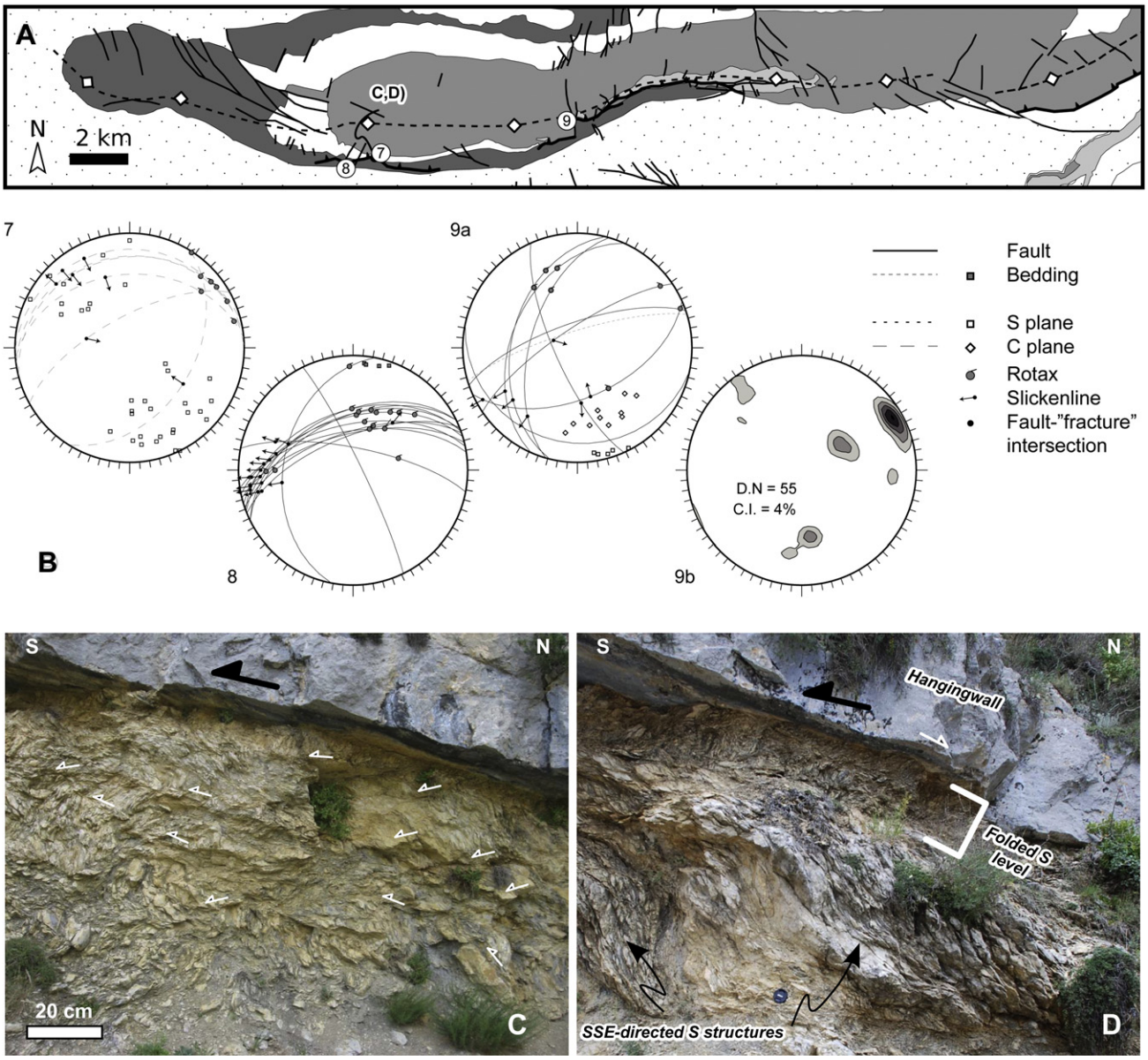

Fig. 4. Map-scale analysis of major thrusts. (A) Location of sites and photos. (B) Stereoplots. In site 7, poles to both S and C planes and slickenlines measured on the C planes are clustered along the NW–SE direction, indicating a top-to-SE shear sense. The same thrust fault is exposed to the west, in site 8. Although the stratigraphic displacement is that of a reverse fault, there the fault slickenlines distribution indicates a top-to-W shear, which clearly represents a younger reactivation of this fault. In site 9 the thrust surface is offset many tens of metres by a normal fault system. Shear sense associated with the thrust is top-to-SE, as both S and C planes are clustered along the NW–SE direction (site 9a). The normal fault zone offsetting the thrust is characterised by the presence of two fault sets striking NNW–SSE (site 9b). The first set includes near-vertical normal faults; the second one includes normal faults dipping about 45° towards the WSW. These two sets, probably being the first one an early joint set later reactivated as normal fault, indicate a WSW–ENE extension direction, as their intersection strikes about NNW–SSE. It is important to remark that this normal fault zone has developed after thrusting, which occurred in the late stages of folding and, accordingly, it represents a late to post-folding structure. (C) S–C and C′ structures within the fault zone of a low-dipping and south-verging thrust in the near-vertical forelimb (site 7). (D) Folded S structures at the top of the shear zone, indicating a later, roughly top-to-N, movement of the thrust (site 7).

rotated projection, where three maxima can be recognised. The main one is near vertical and mostly includes rotaxes of right-lateral faults striking N105° and N130°; the other two maxima are sub-horizontal and strike about 75° (reverse faults) and 110° (normal faults). Veins and joints, in both rotated and unrotated projections, include near-vertical planes striking N160° and, subordinately, N30°. Pressure solution cleavage is the less abundant element, it is at high angle to bedding and strikes from NE–SW to ENE–WSW.

In the syn-rift sediments (Fig. 8e,f) faults are at high angle to bedding and strike: N120°, N140°, N210° and (about) N170°. Rotaxes are strongly scattered. Three broad sub-horizontal maxima are present in both rotated and unrotated analysis, and correspond to directions: NNW–SSE, E–W and NNE–SSW direction. All of them belong to normal faults, with the exception of the E–W striking one that partially includes reverse faults. In the rotated analysis another subvertical maximum can be recognised, corresponding to N120° striking right-lateral strike-slip faults. Few left-lateral strike-slip faults are present, but their poles, slickenlines, and rotaxes are not clustered. Joints and veins are perpendicular to bedding and strike N165° (set 1), N140° (set 2), N20° (set 3) and N85° (set 4) after bedding dip removal. Pressure solution cleavage is, like in the post-rift sediments, the less abundant element. It is near perpendicular to bedding and strikes about ENE–WSW.

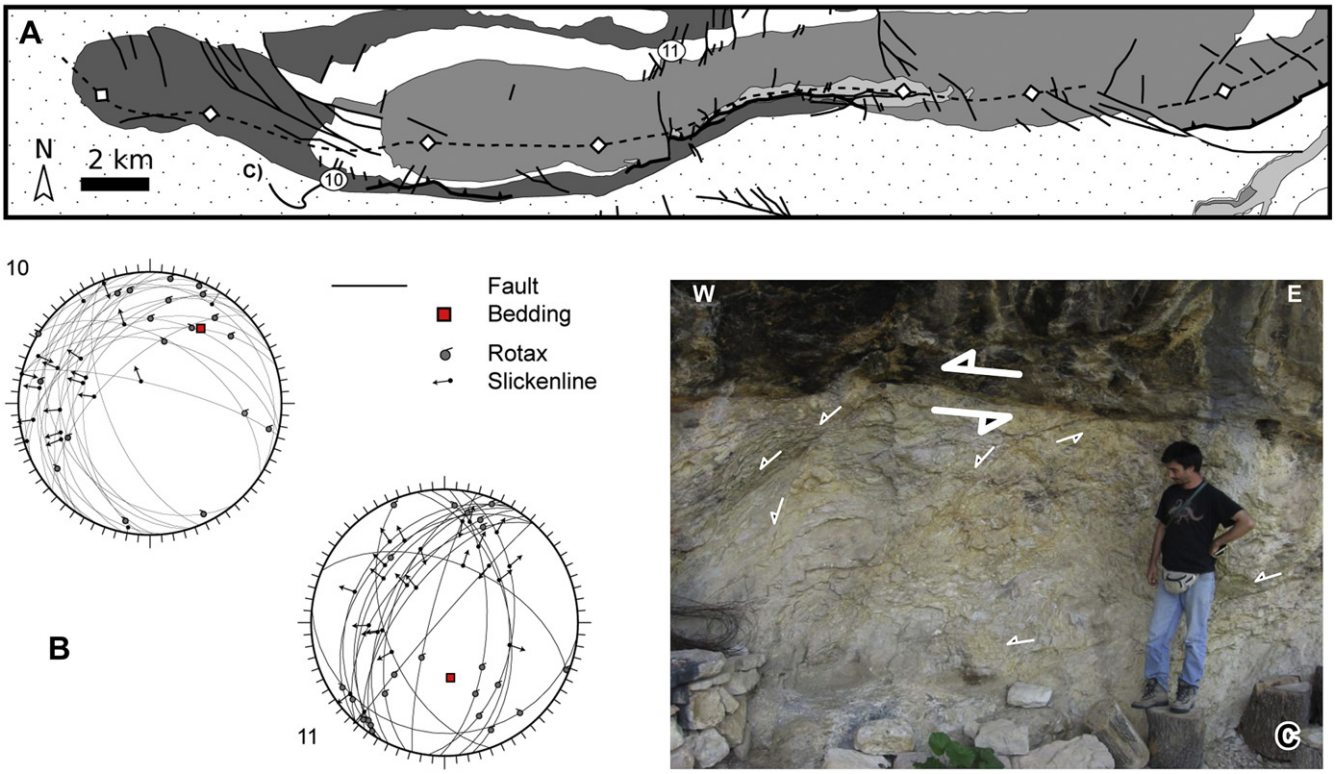

Fig. 5. Map-scale analysis of NNE–SSW striking faults. (A) Location of sites and photos. (B) Stereoplots. In site 10 a low-angle normal fault accomplished for a bulk post-tilting top-to-W hangingwall movement. Fault rotaxes are sub-horizontal, while the bedding surface dips about 50° towards SW. In site 11 extensional mesofaults strike about NNE–SSW, as well as the most part of the fault rotaxes, indicating a WNW–ESE extension direction. The most of fault rotaxes are sub-horizontal and do not lie along the bedding plane, indicating a post-tilting (post-folding) development. Part of the slickenlines are characterised by an NNE direction and a left-lateral strike-slip kinematics, which postdates the extensional event. (C) Low-angle normal fault zone of site 10. Bedding surface is not recognisable.

Finally, Fig. 8g shows the contouring, after bedding dip removal, of slickenlines measured along bedding surfaces and faults forming an angle of less than 15° with the bedding. Although data number is quite limited, an NNW–SSE set is well-recognisable and two other sets striking N–S and NNE–SSW, respectively. All these structures have been observed in the crest and, mostly, in the forelimb. The third set includes elements indicating a top-to-SSW movement. The other two sets include elements indicating a shear sense both top-to-N/NNW (7 data) and top-to-S/SSW (9 data).

The orientation of joints, faults and fault kinematic indicators in both the backlimb and the forelimb are shown in Fig. 9B (displayed in their unfolded attitude). These distributions are characterised by slight differences, which are much more evident when data are grouped according to their along-strike position (Fig. 9C). The orientation of NNW–SSE striking extensional structures does not significantly change along the strike of the study anticline. On the contrary, WNW–ESE and NNE–SSW striking extensional elements (joints, veins and extensional faults) undergo a slight clockwise rotation proceeding towards the east, and in the central sector of the study anticline these elements attain an almost NW–SE and NE–SW strike. Normal faults having NNW–SSE striking rotaxes mostly locate in the central sector, while normal faults having NW–SE striking rotaxes mostly locate to the west. WNW–ESE striking right-lateral faults are found in both areas, but these elements are particularly abundant to the west (i.e. in the WNW–ESE striking fold sector).

4. Cross-cutting relationships

In both syn-rift and post-rift sediments data are better clustered in the unfolded projections (Fig. 8), particularly poles to joints and faults. This indicates that a significant portion of the measured mesostructures developed in response to a stress field having two axes roughly lying on the bedding surface. Accordingly, cross-cutting relationships have to be evaluated firstly by grouping elements having similar strike in the unfolded analysis. Cumulative data analysis and observations in single outcrops indicate that when bedding dip is removed, faults are clustered in three main sets striking WNW–ESE, NNW–SSE, and NNE–SSW. The first one includes both extensional and right-lateral strike-slip faults. Strike-slip slickenlines overprinting WNW–ESE striking extensional assemblages are frequently observed (Fig. 10A,B). NNW–SSE striking faults are normal and a set of joints and veins is oriented parallel to these faults. NNW–SSE striking joints in many places slightly change their orientation approaching WNW–ESE striking elements (Fig. 10C,D), indicating that the former developed after the latter or that the right-lateral reactivation of WNW–ESE striking faults is synchronous to the development of NNW–SSE striking joints. The behaviour of NNE–SSW striking elements is much more complex. In the crest and in the backlimb, ambiguous cross-cutting relationships between joints and veins sets striking NNE–SSW and NNW–SSE are found. Like NNW–SSE striking joints, WSW–ENE striking pressure solution cleavages also change their orientation approaching the WNW–ESE striking elements (Fig. 10E,F), indicating that pressure solution cleavages postdate the WNW–ESE striking elements or, more probably, that cleavage developed rather synchronously to their right-lateral reactivation.

The observed relationships between WSW–ENE striking joints oriented at high angle to bedding and the other elements are as follows. In few places tilted conjugate strike-slip faults are found, suggesting a maximum stress component parallel to bedding and

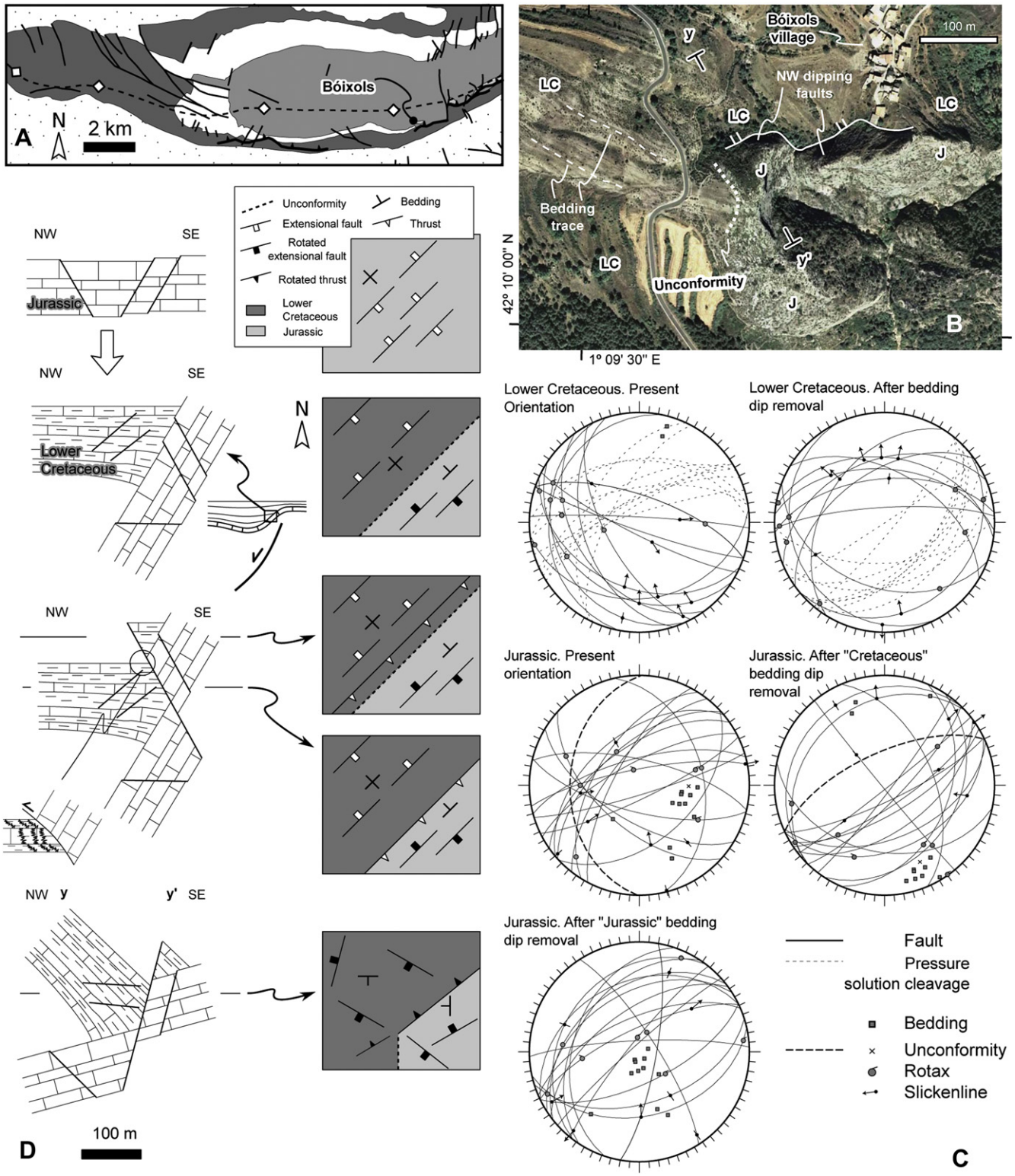

Fig. 6. Inverted extensional transfer fault. (A) Location of the area. (B) Orthophoto of the contact between syn-rift Lower Cretaceous sediments and pre-rift Jurassic limestones. (C) Mesostructural data. In the Lower Cretaceous sediments, the bedding surface strikes about ESE–WNW and dip about 70° towards the south. In the Jurassic limestones bedding surfaces strike from N–S to NNE–SSW and dip is about 40° towards the west. The stratigraphic contact between these units is represented by an onlap surface oriented almost parallel to the bedding surfaces in the Jurassic limestones. The tectonic contact is represented by a system of normal faults striking about NE–SW and dipping towards NW (as seen in B). When the Lower Cretaceous bedding is removed (in both Lower Cretaceous and Jurassic rocks), the orientation of mesostructural elements is the following: pressure solution cleavages found in Lower Cretaceous rocks strike about NE–SW, cleavage is roughly perpendicular to bedding in the marly limestones, while it dips towards SE in the clayish levels; faults in Lower Cretaceous rocks are normal and strike about WSW–ENE; the onlap surface strikes NE–SW and dips towards NW; faults in Jurassic limestones are clustered in two sets, both of them striking NE–SW. The first, major one, includes elements dipping 50–80° towards the SE; the second, sub-ordered one, includes surfaces dipping 10–20° towards NW. When another rotation is applied to the Jurassic dataset, and the onlap surface is restored to the horizontal, these two fault sets again strike NE–SW and their dip is about 50° towards NW and SE, respectively. (D) Cartoon illustrating in cross section and map view the inferred relationships between mesostructures in the syn and pre-rift sediments. The trace of the section (y–y') is shown in (B).

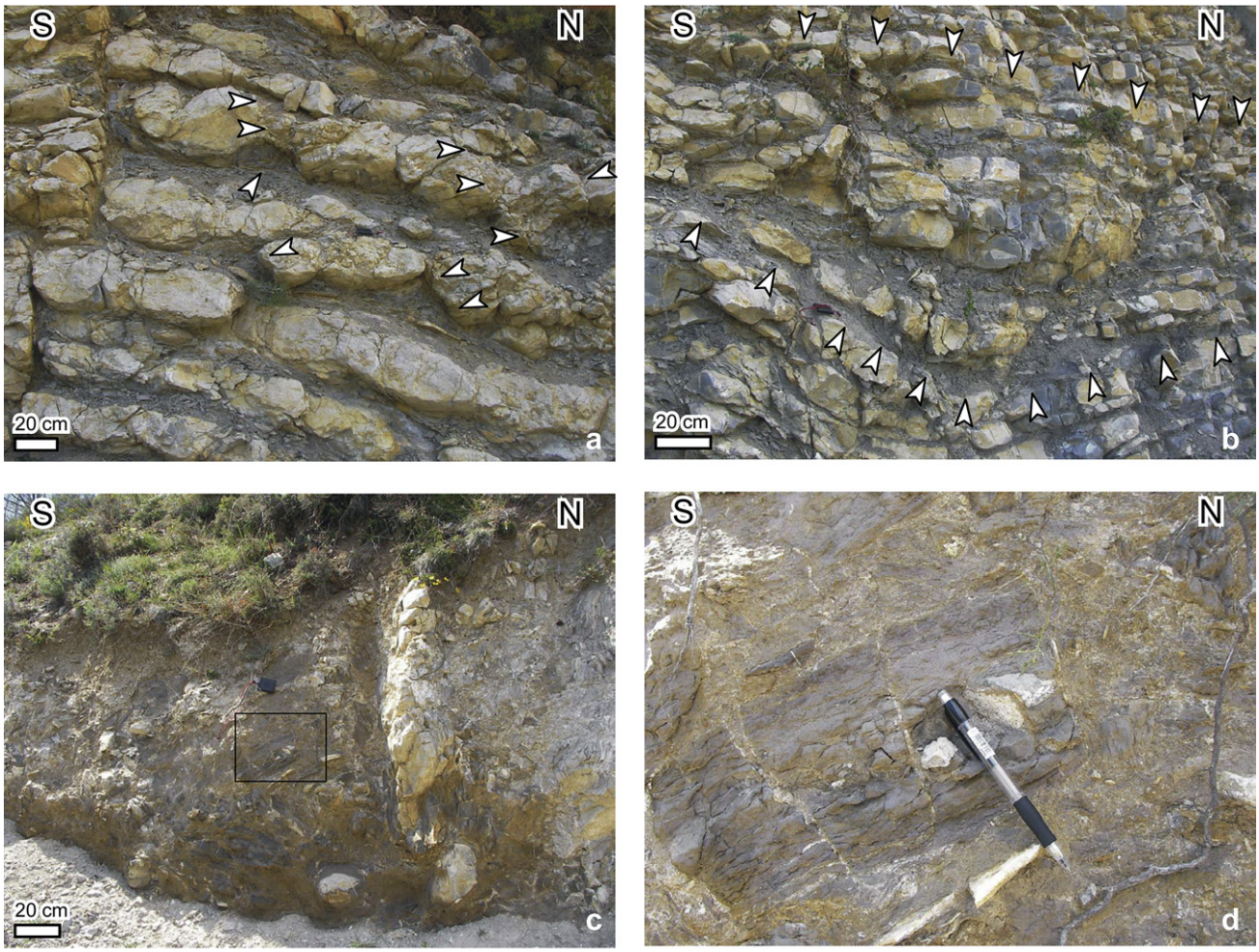

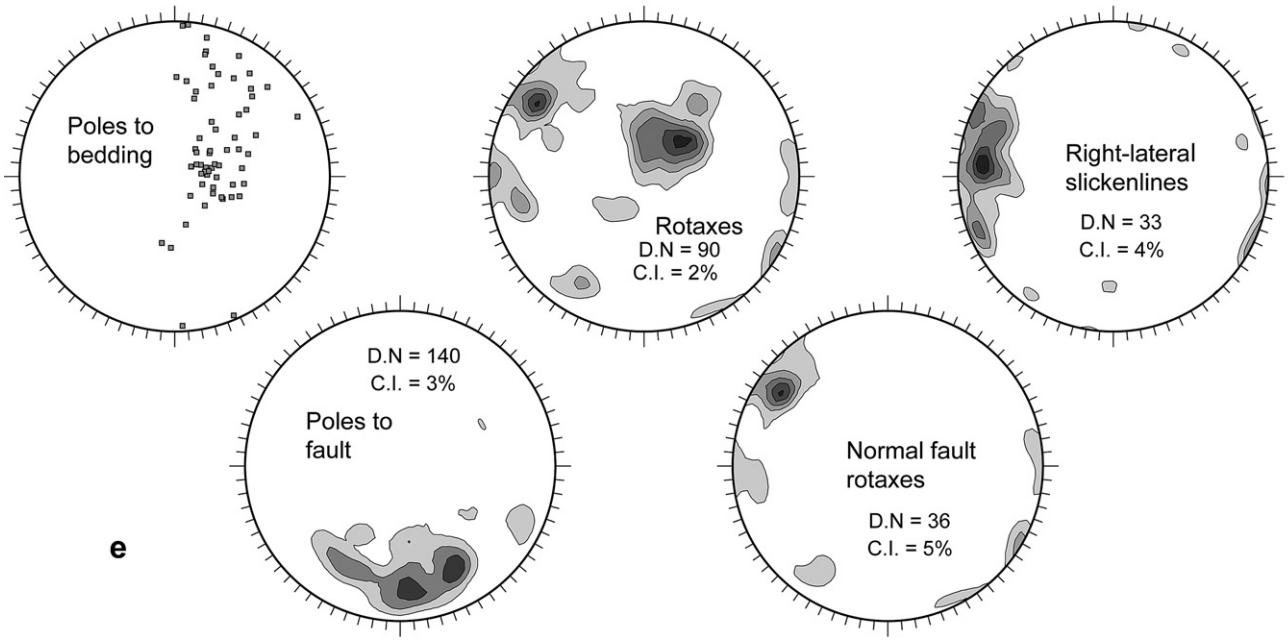

Fig. 7. Early Cretaceous deformation pattern. The site is located 500 m to the east of the Bóixols Village (see Fig. 6A,B for location). (a) Clay injection (indicated by arrows) in the footwall of brittle-ductile domino faults; (b) Syn-extensional growth strata. Arrows indicate top and bottom of the local syn-extensional multilayer. (c) Syn-tectonic slump; (d) Detail of the slump with a clast hosting pre-slump fractures. (e) Mesostructural data. This N–S oriented and 200 m-wide outcrop is characterised by an average bedding dip that, from north to south, passes from sub-horizontal to near vertical. Bedding surfaces strike from E–W to NW–SE. Fault planes strike from NW–SE to NE–SW. The fault rotaxes are clustered around three maxima. Two of them (striking NW–SE and E–W) are sub-horizontal and belong to normal faults. A third major maximum is subvertical and belongs to right-lateral strike-slip faults whose movement direction was WNW–ESE. The strike-slip event postdates the normal one. Soft-sediment deformation structures and growth strata geometries indicate that both the E–W and NW–SE striking faults developed during the Lower Cretaceous extensional event.

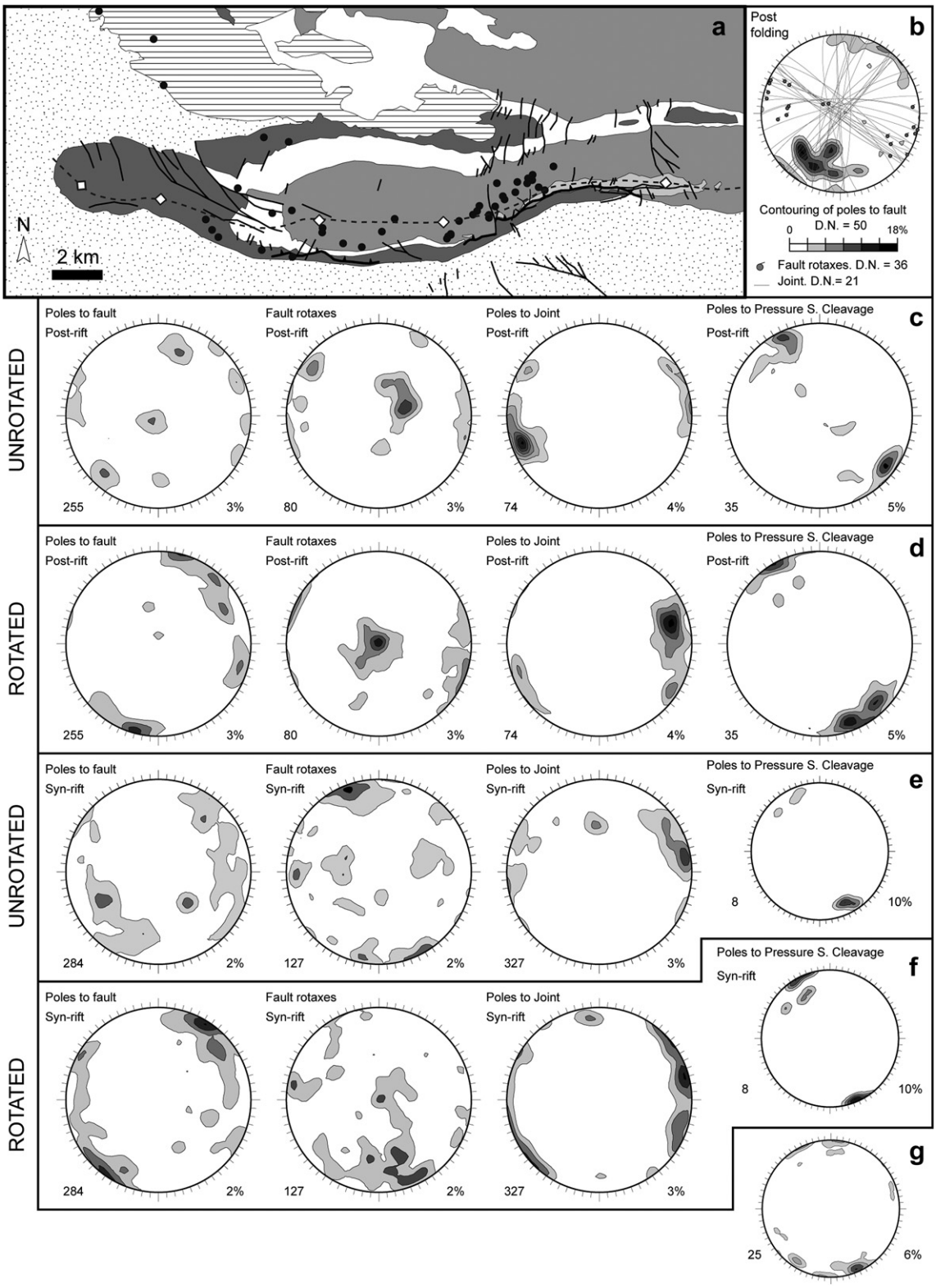

Fig. 8. Mesostructural data analysis. (a) Site locations. (b) Stereoplot of data collected in the post-folding sediments, data are projected after restoring the bedding to the horizontal. Data from the post- (c–d) and syn-rift (e–f) sediments, in their present orientation and after restoring the bedding to the horizontal. (g) Contouring, after bedding dip removal, of slickenlines measured along bedding surfaces and faults at low angle to bedding (<15°).

perpendicular to the WSW–ENE striking pressure solution cleavages. Bedding perpendicular veins striking parallel to the pressure solution cleavages postdate these strike-slip faults (Fig. 11). In other sites we have observed WSW–ENE striking joints arresting on NNW–SSE striking joints, indicating that the former postdate the latter (Fig. 12).

All the above described cross-cutting relationships are between elements at constant angle to bedding, which

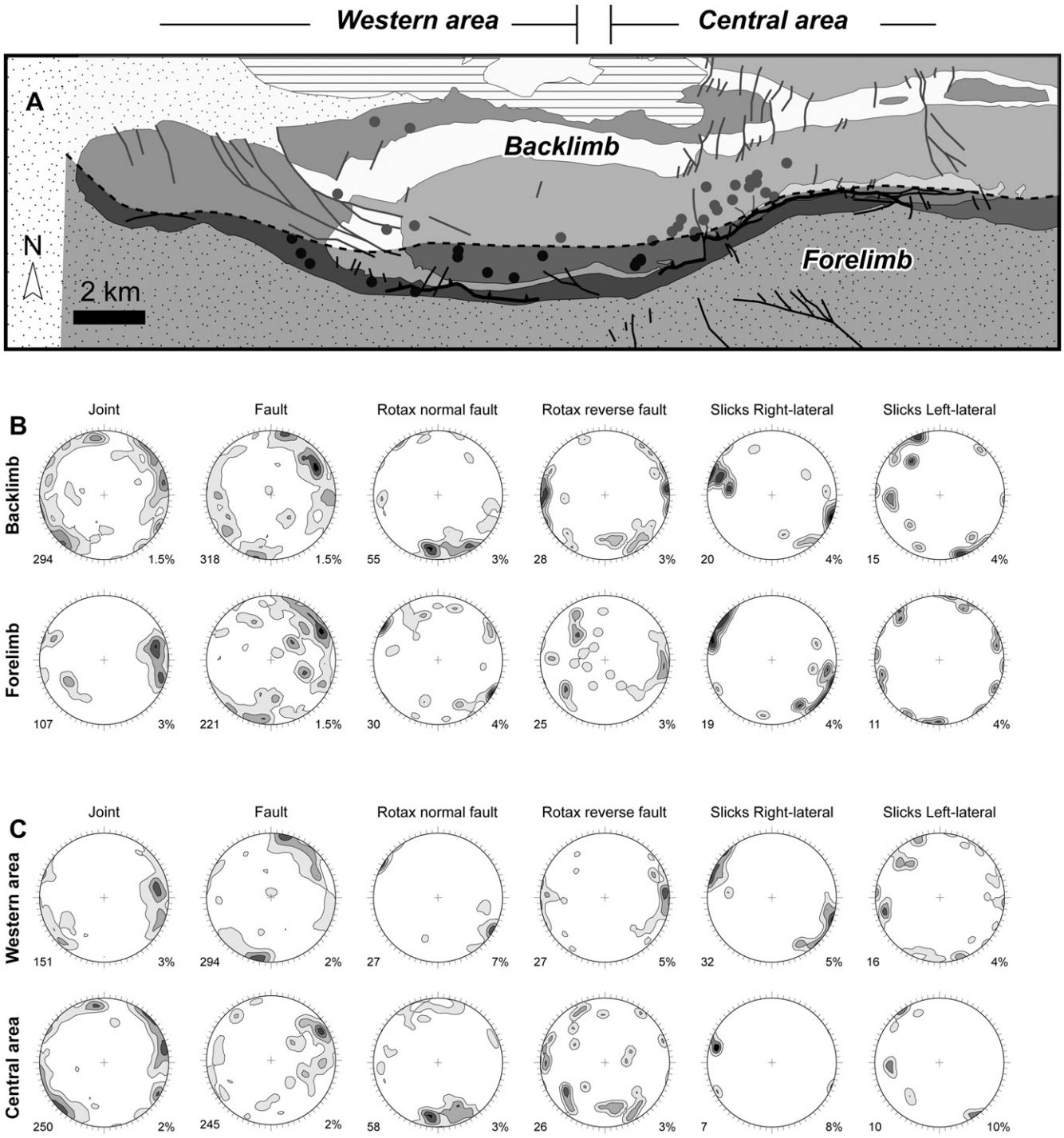

Fig. 9. Mesostructural data, in their unfolded orientation, grouped according to their along and across-strike position. (A) Site locations. (B) Stereoplot of data collected in the backlimb and forelimb. (C) Stereoplot of data collected in the central and western areas.

developed before or in the early stages of the fold growth. There is another set of elements developed in the later stage of folding or after the main folding event. These elements include: low-dipping SSE-verging thrusts in the forelimb and many normal faults striking NNW–SSE, WNW–ESE, and NNE–SSW. As previously reported, the WNW–ESE striking normal faults offset the NNE–SSW striking ones and extensional faults associated with WNW–ESE and NNE–SSW oriented stretching stages postdate thrusts.

5. Discussion

5.1. Structural summary

Presented data are consistent with a scenario including at least three deformation phases (Fig. 13). The younger one is extensional and is responsible for the development of normal faults striking WNW–ESE and of joints striking both WNW–ESE and NNE–SSW (Fig. 13a). The extensional reactivation of the WNW–ESE striking

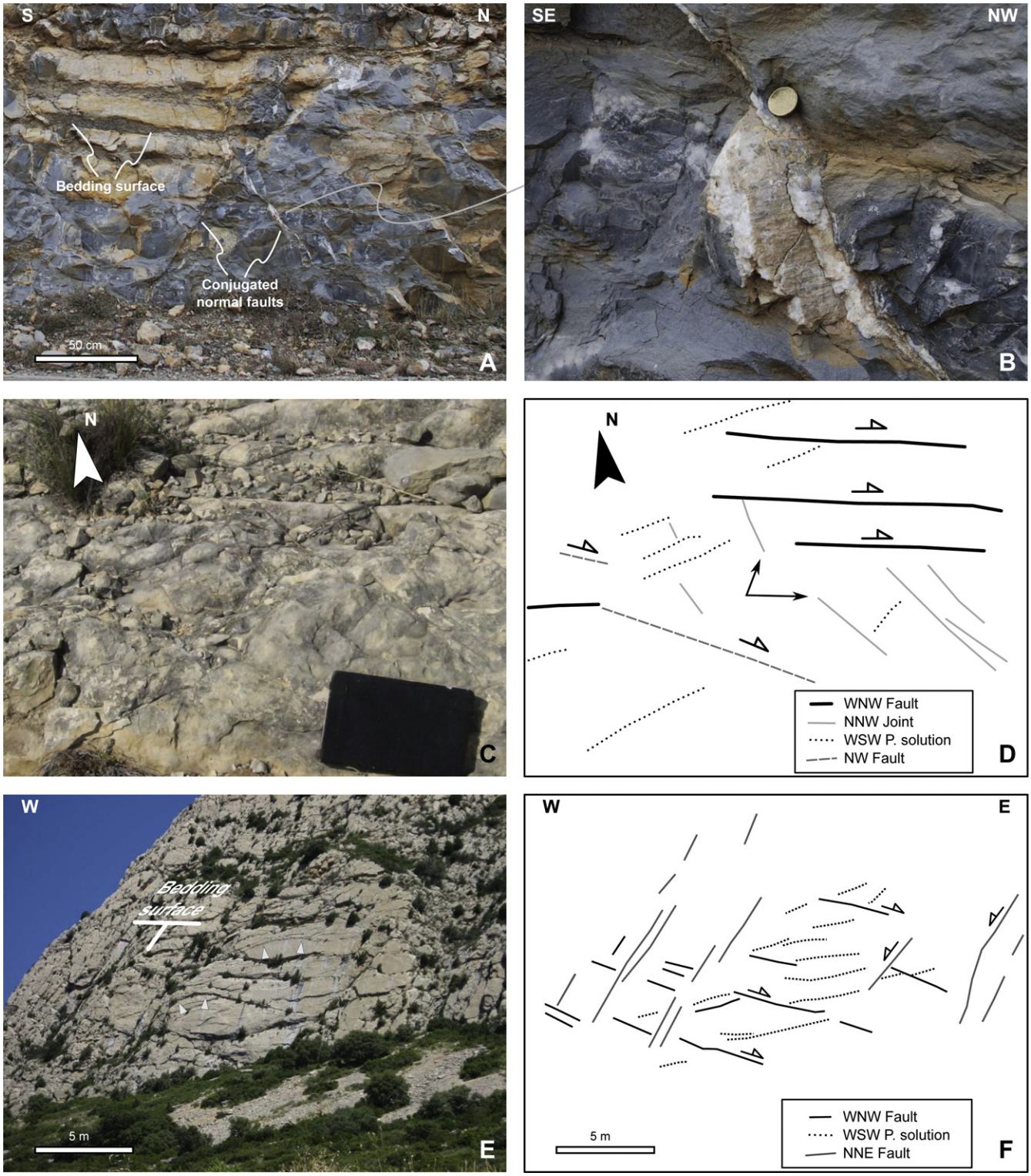

Fig. 10. Examples of cross-cutting relationships. (A–B) Conjugate normal faults reworked as right lateral faults. Lower Cretaceous sediments. (C) Map view and line-drawing (D) of a bedding surface in the post-rift limestones showing WSW–ENE striking pressure solution cleavages and NNW–SSE striking joints delimited by WNW–ESE striking right-lateral faults. Arrows indicate NNW–SSE striking joints changing orientation approaching a WNW–ESE striking element. (E) Photo and line-drawing (F) of a bedding parallel pavement in near-vertical forelimb, post-rift limestones. White arrows indicate pressure solution cleavages changing orientation approaching to tilted right-lateral faults.

fault system located at the transition between the Sant Corneli and Bóixols anticlines is interpreted as related to this stage. This Cenozoic event postdates another extensional event, characterised by an almost perpendicular stretching direction (Fig. 13b), which is responsible for the development of joints, veins and extensional faults striking NNE–SSW. In the backlimb and in the crest this extensional stage led to the development of 50–70°-dipping and NNE–SSW striking normal faults. In the forelimb, extension is achieved by movement along low-angle normal faults and NNE–SSW striking faults (which probably have developed as

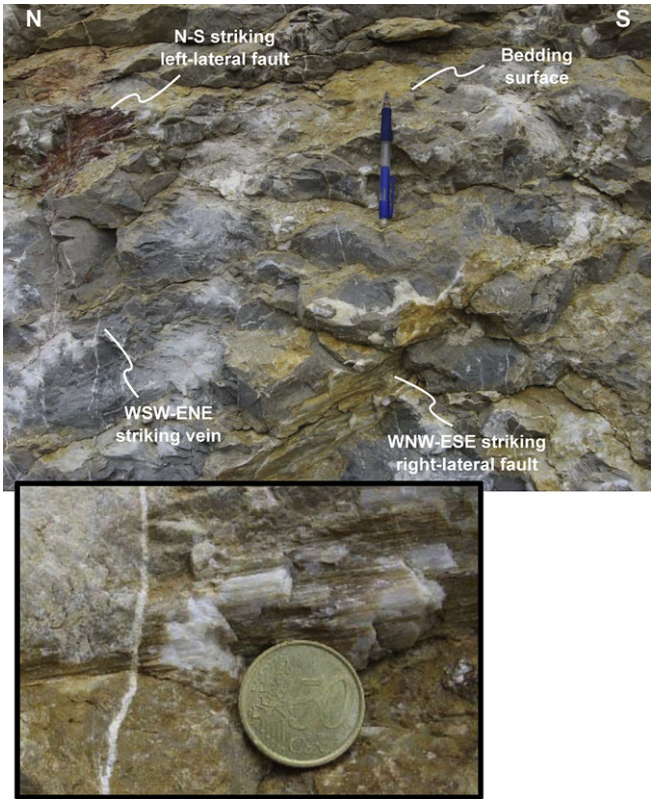

Fig. 11. Photo of WNW–ESE striking right-lateral faults, N–S striking left-lateral fault, and WSW–ENE striking vein postdating a left-lateral fault.

orthogonal joints during the pre-folding extensional stage). As the extensional stages described above are characterised by mutually perpendicular stretching directions, they could be interpreted as a single event: in a first stage $\sigma 3$ and $\sigma 2$ were oriented WNW–ESE and NNE–SSW, respectively (Fig. 13b); in a second later stage an inversion between $\sigma 2$ and $\sigma 3$ would have occurred (Fig. 13a). In the hypothesis that these two events are part of a single deformation stage, a Cenozoic age must be assumed. This suggests that this younger extensional stage could be somehow associated with the Cenozoic reactivation of the study anticline. However, further studies are required to confirm or discard this association.

Once the deformation pattern associated with this extensional event is removed from our dataset, most of the deformation structures in the pre-folding sequence are at a constant angle to bedding. A partial exception to this is represented by few late-folding NNW–SSE striking normal faults, SSE-directed low-dipping thrusts, and near-vertical WNW–ESE striking right-lateral faults. When bedding dip is restored to the horizontal, and late to post-folding elements are removed, the deformation pattern includes (Fig. 14): 1) Joints, veins, and map-scale and mesoscale normal faults striking NNW–SSE; 2) map-scale and mesoscale reverse faults with top to SSE and NNW shear senses and pressure solution cleavages striking ENE–WSW; 3) map scale and mesoscale right-lateral strike-slip faults striking WNW–ESE; 4) faults (mostly right-lateral), joints and veins striking NW–SE; 5) a few NNE–SSW striking left-lateral faults (that, however, could also be post-tilting normal faults); 6) WNW–ESE striking normal faults; 7) NNE–SSW striking normal faults and veins (and subordinately joints) at high angle to bedding; 8) Bedding-perpendicular joints and veins striking WSW–ENE.

Elements of sets from 1 to 5 of Fig. 14 are interpreted as developed during a layer parallel shortening (LPS) event (Fig. 13c), while elements 6 and 7 are interpreted as developed during the pre-folding extensional stage. Pressure solution cleavages and NNW–SSE striking joints are roughly perpendicular and provide layer-parallel $\sigma 1$ and $\sigma 3$, which are oriented about NNW–SSE and WSW–ENE, respectively. Slip directions provided by reverse map-scale faults are consistent with the inferred $\sigma 1$. Slip directions associated with reverse mesofaults range from N–S to NW–SE, which is still consistent with the inferred $\sigma 1$. In this case, data scattering could be associated with the presence of few elements associated with the Cenozoic reactivation of the structure. NW–SE striking right-lateral faults of set 4 are oriented at about 30° from

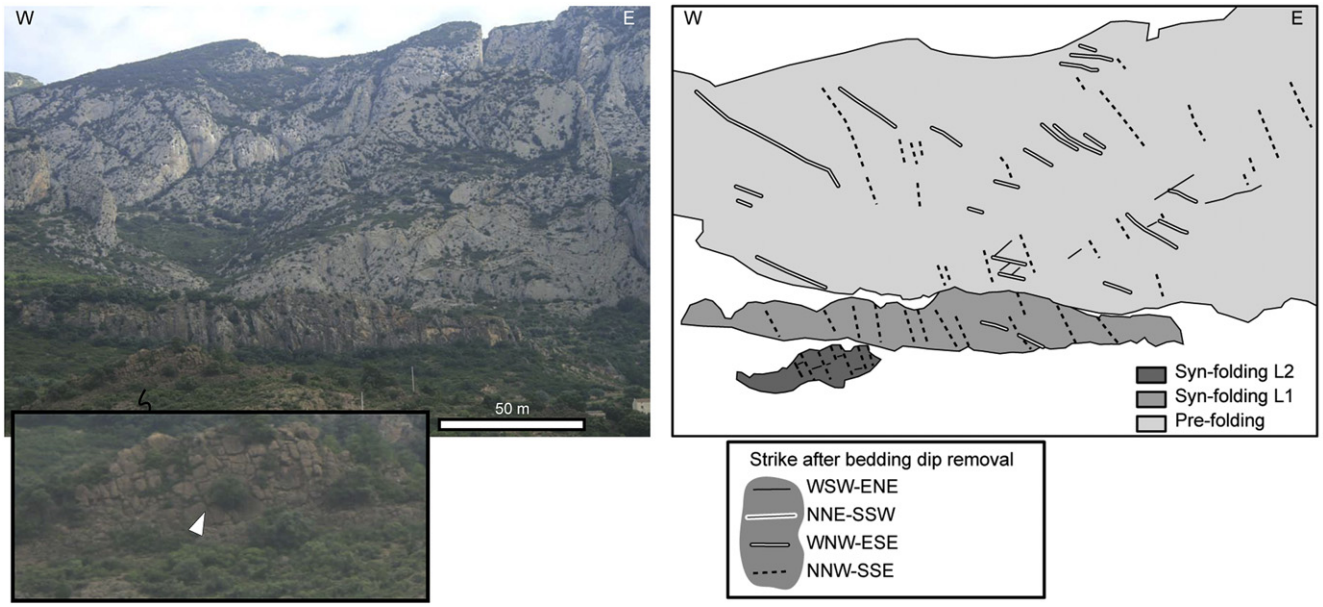

Fig. 12. Photo of pre- and syn-growth layers in the forelimb of the Bóixols anticline, with line-drawing of major fractures. The outcrop is located about 200 m to the west of the Abella de la Conca Village (see Fig. 1 for location). Notice that syn-growth strata are characterised by fractures that, once the bedding dip is removed, strike NNW–SSE and, particularly in the L2 layer, WSW–ENE. White arrow in the inset indicates a WSW–ENE striking joint abutting on NNW–SSE striking joints.

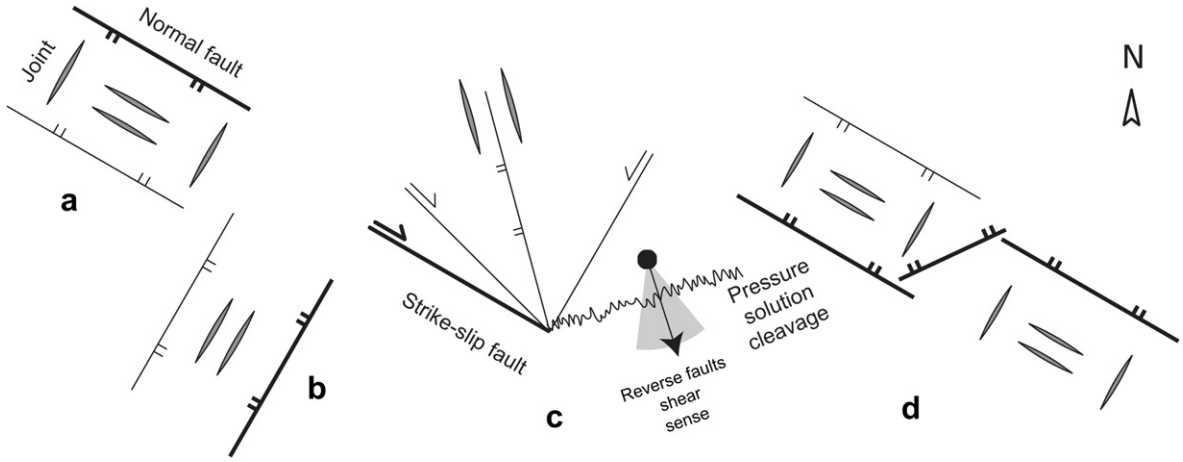

Fig. 13. Scheme illustrating the deformational sequence and the associated mesostructures in the Sant Corneli Bóixols Anticline, from the younger (a) to the older (d) event.

the inferred shortening direction. The parallelism between these right-lateral faults and NW–SE striking joint/vein of set 4 found in the syn-rift sediments allows to interpret part of these joints as small scale right-lateral faults for which it was difficult in the field to recognize the type (i.e. the presence of displacement). However, many of these elements are actually part of the set 6, which is characterised by slightly different orientations in the western (WNW–ESE) and central (NW–SE) portions of the study area (Fig. 9C). Finally, the major elements of the LPS assemblage are the map- and mesoscale WNW–ESE striking right-lateral strike-slip faults (set 3). We interpret them as inherited extensional structures reworked as strike-slip faults due to their favourable orientation with respect to the approximately NNW–SSE oriented shortening direction.

In the framework of an early LPS stage many NNE–SSW striking normal faults located in the near-vertical forelimb could be also interpreted. Many of these structures are near perpendicular to bedding and once the bedding dip is removed they strike NNE–SSW (set 5), i.e. almost perpendicular to the WNW–ESE striking faults. A possible interpretation is that these normal faults are old extensional structures developed orthogonally to the stretching direction during the pre-folding extensional stage. During the LPS stage these elements would have been reworked as left-lateral faults, and later they would have rotated together along with the multilayer.

Grouping structural data with similar strike collected over a large geographic area allows to provide a smoothed and upscaled image of the deformation pattern and, accordingly, of the inferred stress field. However, results provided by this procedure have an intrinsic error and providing a more precise value of the $\sigma 1$ orientation during this layer-parallel shortening stage is not easy. An additional datum allows to fully support the obliquity between Late Cretaceous shortening direction and the E–W trend of the study anticline. The inferred $\sigma 1$ would form an angle of approximately 45° with both WNW–ESE and NNE–SSW striking inherited elements. However, WNW–ESE elements have been abundantly reactivated, while only few NNE–SSW striking left-lateral faults have been measured. Consistently, it must be assumed that the $\sigma 1$ was more optimally oriented for the reactivation of WNW–ESE striking elements, i.e. the angle between $\sigma 1$ and WNW–ESE striking elements was slightly smaller than that between $\sigma 1$ and NNE–SSW striking elements.

A few late-folding elements, i.e. WNW–ESE striking map-scale right-lateral faults located in the eastern sectors of the anticline and the low-dipping SSE-verging thrusts, indicate that the shortening direction was oriented NNW–SSE throughout the entire folding process.

We deduce that the pre-folding extensional stage was characterised by an NNE–SSW oriented stretching direction, and led to the development of WNW–ESE and NNE–SSW striking elements, i.e. sets 6 and 7 of Fig. 14. This idea is supported by the following evidence: (1) cross-cutting relationships indicate that WNW–ESE striking normal faults are reworked as right-lateral faults; (2) syn-sedimentary structures in the Lower Cretaceous sediments indicate a roughly NNE–SSW oriented stretching direction; (3) widespread NNW–SSE striking elements, which include bedding perpendicular joints and veins and rotated normal faults, can be explained by temporary re-orientations of the local stress field induced by failure along WNW–ESE extensional faults, i.e. the mechanisms commonly proposed for the formation of cross-joints (e.g. Gross, 1993; Bai et al., 2002) and/or by invoking along-strike stretching due to differential displacements along laterally terminating WNW–ESE striking Early Cretaceous extensional faults (e.g. Destro, 1995).

Our reconstruction suggests that the Cenomanian to Santonian portion of the multilayer registered the pre-folding extensional deformation. This portion of the multilayer is commonly interpreted as post-rift, as its thickness is roughly constant in the study area (García-Senz, 2002). However, the lack of relevant thickness variations does not necessarily imply the absence of mesoscale extensional deformation associated with the later stages of extensional tectonics and, in particular, with basin subsidence (e.g. Marchegiani et al., 1999).

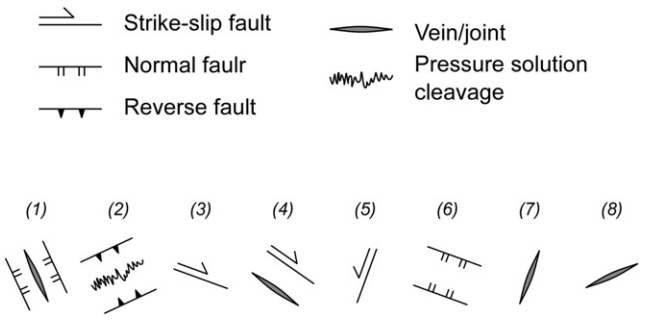

Fig. 14. Scheme showing in map view the mesoscale elements at constant angle to bedding in the study anticline.

The above described scenario does not explain the presence of the few WSW–ENE striking and bedding perpendicular joints and veins (set 8 of Fig. 14). These elements postdate the LPS assemblage (Fig. 11) and have been mostly measured to the east (Fig. 9C), but have been observed also to the east (Fig. 12). As discussed below, according to our interpretation these structures and many almost bedding parallel faults having a top to NNW and SSE shear sense in the forelimb and backlimb, respectively (Fig. 8g), represent the only elements that can be explained by invoking obvious fold-related mechanisms.

Such a reconstruction strongly differs from the model proposed by Shackleton et al. (2011) for the central and western portion of the Sant Corneli Anticline. The discrepancies concern the structural interpretation, not the data. These authors document in the western portion of the Sant Corneli Anticline, the presence of extensional structures striking: NNW–SSE, NNE–SSW, WSW–ENE, and WNW–ESE, which we also measured. In the paper by Shackleton et al. (2011) it is not reported the presence of both WSW–ENE striking pressure solution cleavages and WNW–ESE striking right-lateral faults. However, few mesostructures compatible with these elements have been found in the area (Shackleton, personal communication). The cross-cutting relationships observed by these authors are, partially, similar to what we have observed. NNW–SSE striking extensional structures exhibit ambiguous cross-cutting relationships with the NNE–SSW striking ones. WSW–ENE bedding perpendicular joints postdate the NNW–SSE striking bedding perpendicular joints. The WNW–ESE striking extensional structures postdate the NNE–SSW striking ones. We observe all these cross-cutting relationships but, as previously reported, we also observe NNW–SSE striking joints postdating WNW–ESE striking elements and, above all, we documented the presence of two extensional stages characterised by an NNE–SSW oriented stretching direction, which have developed before and after folding, respectively. The interpretation of Shackleton et al. (2011) is that structures striking NNW–SSE, WNW–ESE and NNE–SSW developed during folding. In the western portion of the Sant Corneli Anticline NNW–SSE and NNE–SSW striking extensional structures mostly locate in the backlimb and forelimb, respectively, forming an angle of about 90° with the local bedding strike. This have been interpreted by Shackleton et al. (2011) as associated with a syn-folding E–W fold axis perpendicular normal faulting initiated early in the folding process, related to uplift and the collapse of the basin margin at the onset of folding. Meso and macrostructures presented in this work indicate that the distribution of NNW–SSE and NNE–SSW striking extensional structures is, in the rest of the Sant Corneli Bóixols Anticline, independent of the bedding strike, which we interpret as being related to the layer-parallel shortening event (NNW–SSE striking structures) and with both pre and post-folding extensional stages (NNE–SSW striking extensional structures).

5.2. Macrostructural evolution

Meso and macrostructural elements hosted in the Sant Corneli Bóixols Anticline have been interpreted as developed during three deformational stages, the Early Cretaceous extensional one being the oldest. As commonly observed in other fold-and-thrust belts (e.g. Coward et al., 1989; Marshak, 2004; Butler et al., 2006; Zanchi et al., 2006), in the studied anticline the post-rift events and the related deformation patterns at different scales are strongly controlled by the geometry of the pre-existing elements.

The data indicate that, during Late Cretaceous inversion, the shortening direction formed an angle of about 65°–70° with the fold axis. Consistently, the Sant Corneli Bóixols Anticline has to be regarded to as an oblique inversion structure. We documented also the existence of an obliquity between the main trend of the Early Cretaceous extensional structures (oriented WNW–ESE) and the fold axis (E–W). A consistent interpretation, which reconciles stratigraphic and structural data, is that the Sant Corneli Bóixols Anticline has developed at the roughly E–W striking eastern termination of a WNW–ESE elongated Lower Cretaceous extensional basin. In this termination the main stretching direction was oriented NNE–SSW, which led to the development of WNW–ESE striking extensional macrostructures and WNW–ESE and NNE–SSW striking mesostructures. Locally transfer faults played an important role in determining the overall geometry of the basin (Fig. 15A). During convergence, transfer faults striking about NE–SW were oriented at high angle to the shortening direction (oriented NNW–SSE) and were reactivated as dip-slip reverse faults (Fig. 15B), like the structure described in Fig. 6. Faults striking WNW–ESE were reactivated, in their deeper portion, in a transpressional setting. In their shallower portions strain was partitioned (e.g. Oldow et al., 1990) between compressive shortcuts and strike-slip fault segments (Fig. 15B). Selective fault linkage during thrust development could have smoothed the geometry of the thrust and, accordingly, that of the anticline.

Data about the anisotropy of magnetic susceptibility (AMS) have been recently published in the area (Gong et al., 2009; Oliva-Urcia et al., 2011). Oliva-Urcia et al. (2011) recognise that the Lower Cretaceous extensional basin was associated with WNW–ESE striking and NNE dipping master faults, which in the study area are oriented about E–W. However, they propose a Lower Cretaceous transtensional kinematics for these faults, to explain the coexistence of magnetic lineations oriented NW–SE, N–S, and NE–SW, all of them acquired, according to these authors, before inversion. Gong et al. (2009) again found a strong data scattering in Lower Cretaceous sediments. Magnetic lineations measured by Gong et al. (2009) strike from NE–SW to N–S, but also NE–SW and about E–W. Gong et al. (2009) conclude that N–S oriented lineations are associated with the N–S oriented Early Cretaceous extension and E–W oriented lineations are associated with N–S directed Late Cretaceous compression.

Our data allow to surely discard the left-lateral transtensional hypothesis proposed by Oliva-Urcia et al. (2011), as no evidences of an important left-lateral strike-slip component were seen along WNW–ESE oriented faults. The apparent discrepancy between AMS and mesostructural data can be reconciled. The scattering of magnetic lineations and their strong spatial variability, coupled with the well-expressed stretching direction provided by mesostructural data, could indicate that AMS data in the Sant Corneli Bóixols Anticline registered early local stretching directions. These would be associated with an early activity of both master and oblique transfer faults, while mesostructural data analysis allows to capture a less local picture of the deformational sequence.

5.3. Folding and fracturing

In the studied anticline, important factors controlling the orientation of mesostructures developed during the inversion stage were: the regional stress field and the inherited mesostructures. The presence of: (1) abundant syn-inversion, pre- to early folding, joints/veins and normal faults striking about NNW–SSE (Fig. 8) and (2) few late-folding NNW–SSE striking extensional structures (Fig. 4 site 6) and WNW–ESE striking right-lateral faults (Fig. 4 sites 4 and 5), indicate that $\sigma 3$ was rather constantly oriented WSW–ENE throughout the entire folding process. The LPS assemblage is interpreted as developed immediately before or in the early stages of folding and represents the bulk of the syn-inversion deformation pattern. In detail, NNW–SSE striking extensional elements of the LPS assemblage are found in the entire structure,

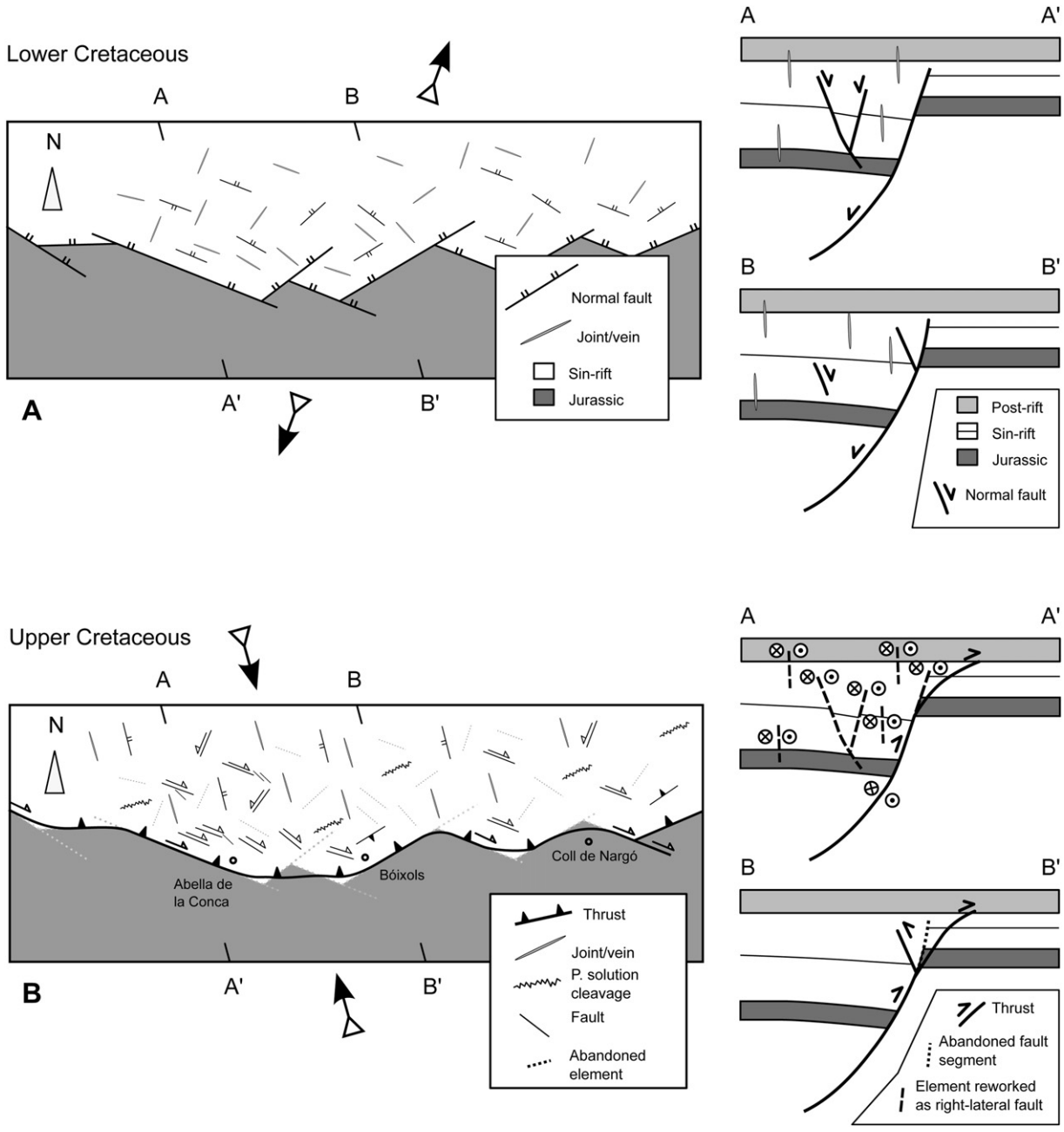

Fig. 15. Map scale and cross sectional views of the deformation pattern associated with Early Cretaceous extension (A) and Late Cretaceous inversion (B).

supporting the idea that part of them has developed before significant folding. On the contrary, the paucity of WNW–ESE striking right-lateral strike-slip faults documented in the E–W (Shackleton et al., 2011) to WSW–ENE striking fold sector (this work), coupled with their abundance in the WNW–ESE striking fold sectors (Fig. 15B), indicates different stress conditions in the different segments of the anticline. From this, it must be deduced that most of the strike-slip reactivation of the inherited Lower Cretaceous extensional elements has occurred during incipient folding, when the ongoing reactivation of the major inherited faults somehow influenced the stress distribution in the hangingwall.

There are few structures that could be interpreted as syn-folding. Bedding perpendicular and WSW–ENE striking joints postdate the LPS pattern, and generally arrest on NNW–SSE striking joints. A possible interpretation is that they have developed perpendicular to a bedding parallel NNW–SSE striking $\sigma 2$, synchronously or slightly after the development of NNW–SSE striking structures that formed perpendicularly to $\sigma 3$, i.e. WSW–ENE striking joints are cross-joints (e.g. Gross, 1993). These WSW–ENE striking extensional structures could relate with a tangential-longitudinal strain, which is expected to induce extension in the outer-arc of the anticline (e.g. Ramsay, 1967). These elements are mostly located in the central sector of the study anticline, where they are parallel to the local fold axis (Fig. 9C). However, although they are less abundant, these structures are found also in WNW–ESE striking western portion of the Bóixols Anticline, where the stretching direction provided by these almost-longitudinal extensional structures is not perpendicular to the fold axial trend, as expected in tangential-longitudinal strain. In particular, the deviation in the WNW–ESE striking fold sectors

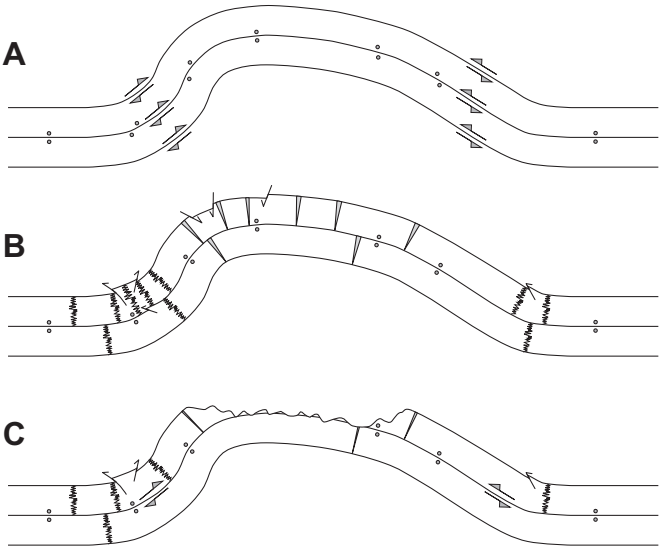

Fig. 16. Mechanisms accommodating fold amplification. (A) Flexural slip. (B) Inner-arc compression and outer-arc extension. (C) Combination of both with syn-folding erosion of the crestal sector. Small circles indicate the amount of layer-parallel displacement.

exceeds 20°. This obliquity further supports the existence of an obliquity between regional shortening direction and fold axis. In fact, the local stress field acting during folding is expected to be the sum of the regional remote stress field and the outer-arc induced stress. As in the WNW–ESE striking fold sectors these components were not coaxial during the growth of the study anticline, the acting stress field is expected to be oblique to both, explaining the non-perpendicularity between fold axial trend and tangential-longitudinal strain induced deformation structures. In all the cases, these almost-longitudinal structures are not widespread and the amount of extension associated with them is quite limited and not sufficient to assume that rock deformation during folding occurred only by tangential-longitudinal strain. We observe few slickenlines along bedding surfaces and along faults at very low angle to bedding (<15°). These mostly strike NNW–SSE and, subordinately, N–S and NNE–SSW. If we assume that slickenlines striking NNE–SSW belongs to layer-parallel segments of pre-folding WNW–ESE striking normal faults, we can assume that the others, which are almost parallel to the inferred regional shortening direction, are associated with flexural-slip. Part of them could have developed during the LPS stage, however, these structures are mostly observed in the forelimb and a significant portion of them has a top-to-the crest shear sense. Consistently, they can be interpreted as associated with flexural-slip folding. Also in the case of flexural-slip we have to assume that the shear sense was not exactly perpendicular to the fold axial trend but, instead, it was oriented much more parallel to the shortening direction. The paucity of structures associated with both tangential-longitudinal strain and flexural-slip could be explained by invoking a syn-growth erosion of the crest with synchronous reverse faulting in the leading syncline. In fact, these processes provide a mechanism that reduces the amount of layer-parallel slip or tangential-longitudinal strain required to fold layers (Fig. 16).

In conclusion, the syn-inversion fracturing of the WNW–ESE striking sectors of the Sant Corneli Bóixols Anticline and its relationships with the hosting fold evolution are the following (Fig. 17). An early layer-parallel shortening event caused the widespread reworking of inherited WNW–ESE oriented elements as right-

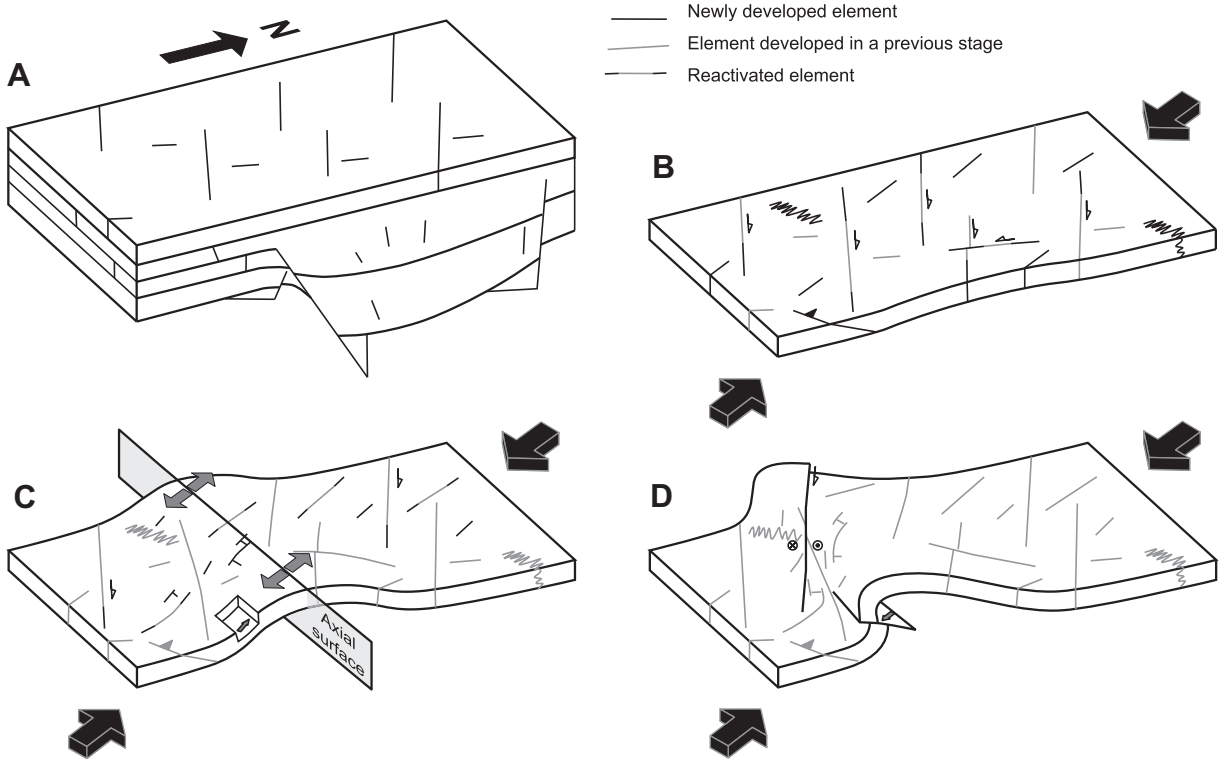

Fig. 17. Cartoon illustrating the relationship between syn-inversion fracturing and fold growth. A) Deformation pattern at the end of the pre-folding extensional stage. B) Layer-parallel shortening stage and incipient folding. Black arrows indicate the shortening direction. C) Syn-folding stage. Flexural-slip shear direction and tangential-pseudo-longitudinal stretching direction are illustrated. D) Fold tightening in the later stage of fold growth.

lateral faults and the development of NNW–SSE oriented extensional structures and WSW–ENE oriented contractional structures. Locally, inherited NNE–SSW striking elements were reworked as left-lateral strike-slip faults (Fig. 17B). Fold amplification was ensured by both flexural-slip and tangential-longitudinal strain (Fig. 17C). Shear sense associated with flexural-slip was parallel to the regional shortening direction. In the outer-arc of the fold, the sum of the stress field induced by tangential-longitudinal strain and the "regional" stress field resulted in a stress field having a $\sigma 2$ striking almost parallel to the regional shortening direction, which led to the development of pseudo-longitudinal extensional structures. In the late stage of folding, fold-tightening related structures developed, including low-dipping thrusts and near-vertical WNW–ESE striking right-lateral faults (Fig. 17D). The same deformational sequence is inferred in the E–W to WSW–ENE striking fold segments. There, however, widespread strike-slip reactivation of inherited mesostructures has not occurred.

6. Conclusions

The Sant Corneli Bóixols Anticline resulted from the oblique inversion of a Early Cretaceous extensional basin. The basin boundary, oriented about E–W, was formed by both faults striking perpendicularly to the stretching direction (oriented WNW–ESE) and transfer faults (roughly oriented NE–SW). During inversion, the shortening direction was oriented NNW–SSE. The fold geometry was forced on that of the basin boundary. In the lower structural levels major extensional faults were reworked with transpressional kinematics, whereas transfer faults were reactivated with an almost pure dip-slip kinematics. In the upper structural levels the inversion-related deformation pattern mostly developed during a Layer-Parallel Shortening stage, which caused the development of extensional and compressional structures striking NNW–SSE and WSW–ENE, respectively, and the right-lateral strike-slip reactivation of previously developed WNW–ESE striking faults. Fold amplification was accommodated by flexural-slip and tangential-longitudinal strain and, probably, by syn-folding erosion of the crestal sector. The few structures associated with these deforming mechanisms are oriented almost perpendicular to the regional shortening direction and oblique to the fold axial trend. Post-folding extensional stage caused the reworking of many structures, with the consequent alteration of cross-cutting relationships.

Acknowledgements

We acknowledge Tom Blenkinsop for the editorial handling. An early version of this manuscript was improved through the critical comments of Ryan Shackleton and of two anonymous reviewers. This work was carried out with the financial support of the TECTOSAL (CGL2010-21968-CO2-01) project, the "Geodinàmica i Anàlisi de Conques (GGAC) research group" (2009SGR-1198) and the Repsol YPF.

References

Anastasio, D.J., Fisher, D.M., Messina, T.A., Holl, J.E., 1997. Kinematics of décollement folding in the Lost River Range, Idaho. Journal of Structural Geology 19, 355–368.

Angelier, J., 1994. Fault slip analysis and paleostress reconstruction. In: Hancock, P.L. (Ed.), Continental Deformation. Pergamon, Oxford, pp. 101–120.

Bai, T., Maerten, L., Gross, M.R., Aydin, A., 2002. Orthogonal cross joints: do they imply a regional stress rotation? Journal of Structural Geology 24, 77–88.

Beamud, E., Garcés, M., Cabrera, L., Muñoz, J.A., Almar, Y., 2003. A new middle to late Eocene continental chronostratigraphy from NE Spain. Earth and Planetary Science Letters 216, 501–514.

Bellahsen, N., Fiore, P., Pollard, D.D., 2006. The role of fractures in the structural interpretation of Sheep Mountain Anticline, Wyoming. Journal of Structural Geology 28, 850–867.

Bergbauer, S., Pollard, D.D., 2004. A new conceptual fold-fracture model including prefolding joints, based on the Emigrant Gap anticline, Wyoming. Geological Society of America Bulletin 116, 294–307.

Bond, R.M.G., McClay, K.R., 1995. Inversion of a Lower Cretaceous extensional basin, south central Pyrenees, Spain. In: Buchanan, J.G., Buchanan, P.G. (Eds.), Basin Inversion. Geological Society Special Publication, vol. 88, pp. 415–431.

Brun, J.P., Nalpas, T., 1996. Graben inversion in nature and experiments. Tectonics 15, 677–687.

Butler, R.W.H., Tavarnelli, E., Grasso, M., 2006. Structural inheritance in mountain belts: an Alpine-Apennine perspective. Journal of Structural Geology 28, 1893–1908.

Casas-Sainz, A.M., 1993. Oblique tectonic inversion and the basement thrusting in the Cameros Massif (Northern Spain). Geodinamica Acta 6, 202–216.

Chester, J.S., 2003. Mechanical stratigraphy and fault-fold interaction, Absaroka thrust sheet, Salt River Range, Wyoming. Journal of Structural Geology 25, 1171–1192.

Chester, J.S., Logan, J.M., Spang, J.H., 1991. Influence of layering and boundary conditions on fault-bend and fault-propagation folding. American Association of Petroleum Geologists Bulletin 103, 1059–1072.

Cooper, M., 1992. The analysis of fracture systems in subsurface thrust structures from the foothills of the Canadian Rockies. In: McClay, K.R. (Ed.), Thrust Tectonics. Chapman and Hall, London, pp. 391–405.

Corbett, K., Friedmean, M., Spang, J., 1987. Fracture development and mechanical stratigraphy of Austin Chalk, Texas. American Association of Petroleum Geologists Bulletin 71, 17–28.

Coward, M.P., Enfied, M.A., Fischer, M.W., 1989. Devonian basins of Northern Scotland: extension and inversion related to Late Caledonian-Variscan tectonics. In: Cooper, M.A., Williams, G.D. (Eds.), Inversion Tectonics. Geological Society Special Publication, vol. 44, pp. 275–308.

Cuevas, J.L., 1992. Estratigrafía del "Garumniense" de la Conca de Tremp. Prepirineo de Lérida. Acta Geológica Hispánica 27, 95–108.

De Sitter, L.U., 1956. Structural Geology. McGraw-Hill, London.

Destro, N., 1995. Release fault: A variety of cross fault in linked extensional fault systems, in the Sergipe-Alagoas Basin, NE Brazil. Journal of Structural Geology 17, 615–629. doi:10.1016/0191-8141(94)00088-H.

Dinares-Turell, J., Garcia-Senz, J., 2000. Remagnetization of Lower Cretaceous limestones from the southern Pyrenees and relation to the Iberian plate geodynamic evolution. Journal of Geophysical Research 105, 19405–19418.

Doblas, M., 1998. Slickenside kinematic indicators. Tectonophysics 295, 187–197.

Donath, F.A., Parker, R.B., 1964. Folds and folding. Geological Society of America Bulletin 75, 45–62.

Engelder, T., 1987. Joints and shear fractures in rock. In: Atkinson, B.K. (Ed.), Fracture Mechanics of Rock. Academic Press, London, pp. 27–29.

Engelder, T., Marshak, S., 1985. Disjunctive cleavage formed at shallow depths in sedimentary rocks. Journal of Structural Geology 7, 327–342.

Engelder, T., Peacock, D.C.P., 2001. Joint development normal to regional compression during flexural-flow folding: the Lilstock buttress anticline, Somerset, England. Journal of Structural Geology 23, 259–277.

Fischer, M.P., Jackson, P.B., 1999. Stratigraphic controls on deformation patterns in fault-related folds: a detachment fold example from the Sierra Madre Oriental, northeast Mexico. Journal of Structural Geology 21, 613–633.

Fletcher, R.C., Pollard, D.D., 1981. Anticrack model for pressure solution surfaces. Geology 9, 419–424.

García-Senz, J., 2002. Cuencas extensivas del Cretacico Inferior en los Pirineos Centrales, formación y subsecuente inversión. PhD thesis, Barcelona University. 310 pp.

Gong, Z., Van Hinsbergen, D.J.J., Vissers, R.L.M., Dekkers, M.J., 2009. Early Cretaceous syn-rotational extension in the Organya basin – new constraints on the palinspastic position of Iberia during its rotation. Tectonophysics 473, 312–323.

Gross, M.R., 1993. The origin and spacing of cross joints: examples from the Monterey Formation, Santa Barbara Coastline, California. Journal of Structural Geology 15, 737–751.

Gross, M.R., 1995. Fracture partitioning: failure mode as a function of lithology in the Monterey Formation of coastal California. Geological Society of America Bulletin 107, 779–792.

Hancock, P.L., 1985. Brittle microtectonics: principles and practice. Journal of Structural Geology 7, 437–457.

Jamison, W.R., 1992. Stress controls of fold thrust style. In: McClay, K.R. (Ed.), Thrust Tectonics. Chapman and Hall, London, pp. 155–164.

Lanaja, J.M., 1987. Contribución de la exploración petrolífera al conocimiento de la geología de España, vol. 465. Instituto Geológico y Minero de España, Madrid.

Lemiszki, P.J., Landes, J.D., Hatcher Jr., R.D., 1994. Controls on hinge-parallel extension fracturing in single-layer tangential-longitudinal strain folds. Journal of Geophysical Research 99, 22027–22042.

Marchegiani, L., Bertotti, G., Cello, G., Deiana, G., Mazzoli, S., Tondi, E., 1999. Pre-orogenic tectonics in the Umbria-Marche sector of the Afro-Adriatic continental margin. Tectonophysics 315, 123–143.

Marshak, S., 2004. Salients, recesses, arcs, oroclines, and syntaxes: a review of ideas concerning the formation of map-view curves in fold-thrust belts. In: McClay, K.R. (Ed.), Thrust Tectonics and Hydrocarbon Systems. Memoir of the American Association of Petroleum Geologists, vol. 82, pp. 131–156.

Mencos, J., 2011. Metodologies de reconstrucció i modelització 3D d'estructures geològiques: anticlinal de Sant Corneli–Bóixols (Pirineus Centrals). PhD thesis, Barcelona University.
Mitra, G., Yonkee, W.A., 1985. Relationship of spaced cleavage to fold and thrust in the Idaho-Utah-Wyoming thrust belt. Journal of Structural Geology 7, 361–373.
Muñoz, J.A., 2002. Alpine tectonics I: the Alpine system north of the Betic Cordillera: the Pyrenees. In: Gibbons, W., Moreno, T. (Eds.), The Geology of Spain. Geological Society of London Special Publication, pp. 370–385.
Oldow, J.S., Bally, A.W., Ave Lallemant, H.G., 1990. Transpression, orogenic float, and lithospheric balance. Geology 18, 991–994.
Oliva-Urcia, B., Casas, A.M., Soto, R., Villalaín, J.J., Kodama, K., 2011. A transtensional basin model for the Organyà basin (central southern Pyrenees) based on magnetic fabric and brittle structures. Geophysical Journal International 184, 111–130.
Pollard, D.D., Aydin, A., 1988. Progress in understanding jointing over the past century. Geological Society of America Bulletin 100, 1181–1204.
Price, N.J., Cosgrove, J.W., 1990. Analysis of Geological Structures. Cambridge University Press, Cambridge.
Ramsay, J.G., 1967. Folding and Fracturing of Rocks. McGraw-Hill, New York.
Ramsay, J.G., 1974. Development of chevron folds. Geological Society of America Bulletin 85, 1741–1754.
Savage, H.M., Shackleton, J.R., Cooke, M.L., Riedel, J.J., 2010. Insights into fold growth using fold-related joint patterns and mechanical stratigraphy. Journal of Structural Geology 32, 1466–1475.
Shackleton, J.R., Cooke, M.L., Verges, J., Simo, T., 2011. Temporal constraints on fracturing associated with fault-related folding at Sant Corneli anticline, Spanish Pyrenees. Journal of Structural Geology 33, 5–19.
Simó, A., 1986. Carbonate platform depositional sequences, Upper Cretaceous, south-central Pyrenees (Spain). Tectonophysics 129, 205–231.
Srivastava, D.C., Engelder, T., 1990. Crack-propagation sequence and pore-fluid conditions during fault-bend folding in the Appalachian Valley and Ridge, central Pennsylvania. Geological Society of America Bulletin 102, 116–128.
Stearns, D.W., 1968. Certain aspect of fracture in naturally deformed rocks. In: Rieker, R.E. (Ed.), National Science Foundation Advanced Science Seminar in Rock Mechanics. Special Report. Air Force Cambridge Research Laboratories, Bedford, MA, pp. 97–118. AD66993751.
Suppe, J., 1983. Geometry and kinematics of fault-bend folding. American Journal of Science 283, 684–721.
Tavani, S., Storti, F., Fernández, O., Muñoz, J.A., Salvini, F., 2006. 3-D deformation pattern analysis and evolution of the Añisclo anticline, southern Pyrenees. Journal of Structural Geology 28, 695–712.
Tavani, S., Storti, F., Salvini, F., Toscano, C., 2008. Stratigraphic versus structural control on the deformation pattern associated with the evolution of the Mt. Catria anticline, Italy. Journal of Structural Geology 30, 664–681.
Tavani, S., Storti, F., Munoz, J.A., 2010. Scaling relationships between stratabound pressure solution cleavage spacing and layer thickness in a folded carbonate multilayer of the Northern Apennines (Italy). Journal of Structural Geology 32, 278–287.
Thomas, D.W., Coward, M.P., 1995. Late Jurassic-Early Cretaceous inversion of the northern east Shetland Basin, northern North Sea. In: Buchanan, J.G., Buchanan, P.G. (Eds.), Basin Inversion. Geological Society Special Publication, vol. 88, pp. 275–306.
Turcotte, D.L., Schubert, G., 1982. Geodynamics: Applications of Continuum Physics to Geological Problems. Wiley and Sons, New York, 450 pp.
Wise, D.U., Vincent, R.J., 1965. Rotation axis method for detecting conjugate planes in calcite petrofabric. American Journal of Science 263, 289–301.
Zanchi, A., Berra, F., Mattei, M., Ghassemi, M.R., Sabouri, J., 2006. Inversion tectonics in central Alborz, Iran. Journal of Structural Geology 28, 2023–2037.